



Research Article

Modulation Instability and Novel Exact Soliton Solutions of the Nonlocal Kundu-Eckhaus Equation

Md Alamgir Hossain¹, Md. Nur Alam^{2,3,4}, Shams Forruque Ahmed^{2,5*} , Cemil Tunç⁶ 

¹Department of Mathematics, Govt. Edward College, Pabna, 6600, Bangladesh

²School of Mathematical Sciences, Sunway University, Bandar Sunway, Petaling Jaya, Selangor Darul Ehsan, 47500, Malaysia

³Department of Mathematics, Pabna University of Science and Technology, Pabna, 6600, Bangladesh

⁴Department of Mathematics, Saveetha School of Engineering, Saveetha Institute of Medical and Technical Sciences, Chennai, Tamilnadu, 602105, India

⁵Miyan Research Institute, International University of Business Agriculture and Technology, Dhaka, Bangladesh

⁶School of Engineering and Natural Sciences, Istanbul Medipol University, Istanbul, 34810, Turkey

E-mail: shams.forruque@northsouth.edu

Received: 12 August 2025; **Revised:** 16 September 2025; **Accepted:** 16 September 2025

Abstract: Diverse fields of modern science, including mathematical modeling and physics, plasma physics, atmospheric sciences, marine sciences, hydrodynamics, nonlinear mechanics, and other complex nonlinear physical phenomena, are expressed through Nonlinear Partial Differential Equations (NLPDEs). Exact solutions play an important role in understanding the behavior of solitary wave solutions and the dynamical properties of significant outcomes for higher-dimensional NLPDEs. As an integrable extension of the nonlinear Schrödinger equation, the nonlocal Kundu-Eckhaus model comprehends higher-order nonlinearities and nonlocal effects. The stability properties of dark, bright, periodic multiple, and singular soliton solutions to the nonlocal Kundu-Eckhaus (KE) equation within the Parity-Time (PT) symmetry model are studied here, whereas past studies have neglected the effects of nonlocal interactions and PT symmetry. $\frac{AG'}{GE}$ is a well-established method, particularly for depicting wave dynamics in nonlinear optical and quantum systems. We attain exact traveling wave solutions evolved in hyperbolic and trigonometric forms, representing several classes of solitons by applying this method. The findings elucidate that the obtained soliton solutions are stable under small perturbations, highlighting their robustness and the persistence of localized waveforms in nonlocal circumstances. We plotted 3D, 2D, and contour graphs for simulating our findings using MATLAB. This research sheds light on the mysterious understanding of nonlocal nonlinear wave behaviors and offers analytical methodologies for future scrutiny in fields such as optical physics and complex nonlinear systems.

Keywords: nonlinear optics, nonlinear Kundu-Eckhaus equation, analytical method, Modulation Instability (MI)

MSC: 35E05, 35C08, 35Q51, 37L50, 37J25, 33F05

1. Introduction

Nonlinear Partial Differential Equations (NLPDEs) are widely used as models to explain complex physical events in a range of natural science domains, as many natural processes are inherently nonlinear. NLPDEs are a special class of

Nonlinear Evolution Equations (NLEEs) that describe intricate physical processes in diverse scientific and engineering fields. These equations link variables and their derivatives to effectively describe complex physical processes such as fluid flow, plasma behavior, turbulence, climate modeling, financial modeling, optical transmission, materials science, neurology, biology, and quantum effects. They achieve this by capturing how waves propagate, interact, and transfer energy in nonlinear systems [1]. Nonlocal nonlinear equations are a relatively new family of integral equations that have achieved considerable attention in recent decades due to their unique properties in nonlinear complex dynamic systems [2]. Ablowitz et al. introduced an integrable nonlocal nonlinear Schrödinger equation in 2013 [3]. This equation arises from a symmetry reduction of the AKNS hierarchy and is related to a Parity-Time (PT)-symmetric framework by Bender and Boettcher [4–6]. Numerous nonlocal integrable equations for potential applications in nonlinear PT-symmetric media have been derived from the AKNs scattering framework [7–9]. PT-symmetry concepts have been studied in plasmonics, optical meta-materials, and coherent atomic media [10–13]. The absorption system is applied in PT-symmetric optical structures to improve wave behavior, imaging, and sensing, thereby transforming limitations into useful features. In simpler terms, when the balance between gain and loss is reached, the PT-symmetric index profile maintains a fully real mode. This balance allows light to move smoothly even with strong gain and loss. Several researchers have neglected the influence of nonlocal interactions and PT symmetry despite the extensive development of analytical methods for NLPDEs, focusing instead on classical nonlocal models. This paper presents the nonlocal Kundu-Eckhaus (KE) equation, which extends the nonlinear Schrödinger model with higher-order nonlinearities. In contrast, a nonlocal form with reverse-space and time coupling PT-symmetric represents a deviation from the classical model. It models the transmission of optical solitons through birefringent fibers [14]. However, limited attention has been given to validating the physical relevance of obtaining soliton solutions through Modulation Instability (MI). Moreover, numerous investigations do not explicitly address in nonlocal media how PT symmetry modifies the soliton interactions. As a consequence, sufficient connections between exact analytical solutions and physical relevance regarding MI in PT-symmetry remain unexplored. In plasma physics and quantum optics, the designed equation could be extended where nonlocal and PT-symmetric interactions are increasingly relevant. In this paper, our applied $\frac{AG'}{GE}$ method provides exact solutions to the PT-symmetric nonlocal KE equation in nonlinear optical systems, which are physically meaningful under MI [15]. Our method and its variants provide a systematic approach to deriving exact solutions for complex nonlinear problems. In particular, we examine how cubic and quartic nonlinearities along with self-frequency shift in the nonlocal nonlinear KE equation, influence the MI of optical solitons in a birefringent fiber. This study introduces and solves a physically rich version of the nonlocal nonlinear Kundu-Eckhaus equation with the PT-symmetry model. However, most previous research has focused either on the local KE equation or its nonlocal version without incorporating PT-symmetry. On the other hand, PT-symmetric extensions of nonlinear models are known to capture realistic gain-loss balance in optical systems and to yield novel spectral and stability properties. Despite their individual importance, a unified treatment of nonlocality and PT-symmetry within the KE framework has not been systematically investigated. This gap is particularly significant because combining these two features may reveal richer soliton dynamics in birefringent fibers and PT-symmetric optical waveguides. Removing the limitations of existing literature, our obtained solutions established an analytical framework for understanding how PT-symmetry, nonlocality, and higher-order effects interact, offering new theoretical tools for controlling and predicting nonlinear wave behavior. Our proposed method provides a novel framework for obtaining exact solutions of nonlocal integrable equations extending the scope of classical techniques. While the Hirota bilinear method, Darboux transformation, and Riemann-Hilbert problem are effective for local integrable systems, they often face limitations such as difficult bilinearization, dependence on seed solutions, or complex analytic procedures. In contrast, the present approach directly generates exact solutions for nonlocal KE equations, offering a simpler, more flexible, and wider range of applicable frameworks. Validation is achieved analytically by recovering known solutions, where applicable, and numerically through simulations that confirm solution stability and evolution. Compared to existing methods, the applied $\frac{AG'}{GE}$ method reduces algebraic complexity and computational effort. Overall, the method demonstrates both efficiency and robustness, highlighting its novelty and practical significance in the study of nonlocal integrable systems.

The remaining sections of this paper are designed as follows. We described related works in Section 2. In Section 3, named related works, we show the procedure for the nonlocal KE equation. In Section 4, we include the results of our

proposed equation. The interpretation of the graphical representation of our desired solution is provided in Section 5. In Section 6, the analysis of MI is presented. Comparisons to other methods are in Section 7, the conclusions and future are in Section 8.

2. Related works

Over the years, many authors have studied the solution of different nonlinear evolution equations using other methods. Zhou et al. used the Hirota bilinear method which is a powerful method for obtaining multi-soliton solutions to integrable partial differential equations [16]. It transforms nonlinear equations into bilinear forms. Using pairs of conjugate wave variables in the $2N$ -soliton solutions generates N -complexion solutions and facilitates the identification of soliton solutions through perturbative expansions. While Riaz et al. presented the Darboux transformation for a semi-discrete matrix coupled dispersionless system for generating new soliton solutions from known ones by proposing a Lax pair, particularly useful in the context of integrable systems [17]. The Riemann-Hilbert problem involves finding a pair of analytic functions that satisfy certain boundary conditions, provides a systematic approach to solving integrable systems and is applicable to a wide range of problems in mathematical physics [18]. Besides these methods, numerous methods have been applied for finding exact soliton solutions of partial differential equations such as the inverse scattering transform [19], (G'/G) expansion process [20], similarity transformation [21], Lie symmetry analysis [22], tanh-coth process [23], Jacobi elliptic function process [24], unified technique [25], Painlevé analysis [26], modified exp-function process [27], $(1/G)$ -expansion process [28], generalized projective riccati equation process [29], homogeneous balance process [30], ansatz technique [31], direct algebraic procedure [32], improved F -expansion scheme [33], new extended direct algebraic process [34], extended tanh expansion scheme [35], modified Kudryashov process [36], sine-Gordon expansion scheme [37], invariant subspace process [38], Sardar sub-equation scheme [39], modified simple equation algorithm [40] and so on. Khuri et al. investigated the four types of nonlinear terms in Kudryashov's equation in bright, dark, and single optical soliton solutions [41]. MI in nonlinear wave systems describes how minor disturbances enlarge over time, leading to the emergence of new patterns [42]. MI is essential in optics, wave propagation, and the fields of fluid dynamics [43]. These studies have overlooked the crucial effects of higher-order nonlinear terms, which are essential in modern physics for capturing the exact solutions of complex dynamics.

3. Materials and methods

3.1 Outline of the adapted (G'/G) -expansion method

Consider the NLPDE in the general form

$$\psi(Z_t, Z_x, Z_{xx}, Z_{yy}, Z_{xyy}, \dots) = 0. \quad (1)$$

In Eq. (1), ψ is a polynomial function of the dependent variables and all of its derivatives. We now discuss the main stages of the $\left(\frac{AG'}{GE}\right)$ -expansion method.

Step 1 Analyze the wave transformation as (2).

$$Z(x, y, t) = Z(\vartheta), \quad \vartheta = x - vt. \quad (2)$$

We obtain the ordinary differential equation for Eq. (1) as

$$\phi(-vZ', Z', Z'', Z''', \dots) = 0. \quad (3)$$

Here ϕ is a polynomial function of $Z(\vartheta)$ and its derivatives.

Step 2 The solution for Eq. (3) in a series form is given as

$$Z(\vartheta) = \sum_{-N}^N K_i S^i, \quad (4)$$

where $S = \left(\frac{G'}{G} + \frac{\lambda}{2} \right)$, $|K_{-N}| + |K_N| \neq 0$ and $G = G(\varphi)$ fulfills the relation

$$G'' + \lambda G' + \mu G = 0, \quad (5)$$

where $K_i (\pm 1, \pm 2, \pm 3, \dots, \pm N)$. From Eq. (4), we induce

$$S' = r - S^2. \quad (6)$$

Therefore, S satisfies Eq. (6) as (7)

$$S = \begin{cases} \sqrt{r} \tanh(\sqrt{r}\vartheta), r > 0. \\ \sqrt{r} \coth(\sqrt{r}\vartheta), r > 0. \\ \frac{1}{\vartheta}, r = 0. \\ -\sqrt{-r} \tan(\sqrt{-r}\vartheta), r < 0. \\ \sqrt{-r} \cot(\sqrt{-r}\vartheta), r < 0. \end{cases} \quad (7)$$

Where $r = \frac{\lambda^2 - 4\mu}{4}$ and r is considered employing λ and μ .

3.2 Methodology

The study begins with the formulation of a nonlocal integrable equation with specified parameters and boundary conditions. A direct analytical method is then applied to transform the nonlocal terms into a solvable form, from which exact soliton, dark soliton, and periodic solutions are derived and verified. These results are validated through comparison with established techniques such as the Hirota bilinear method, Darboux transformation, and Riemann-Hilbert problem. Numerical simulations further examine stability and dynamic behavior confirming both mathematical soundness and physical relevance. In this study, we developed a nonlocal KE equation model recently solved by the Hirota bilinear

method, yielding an N-soliton solution by Deng et al. [43]. To understand the solution procedure of the nonlinear PDE, a flow chart is given of $\frac{AG'}{GE}$ method.

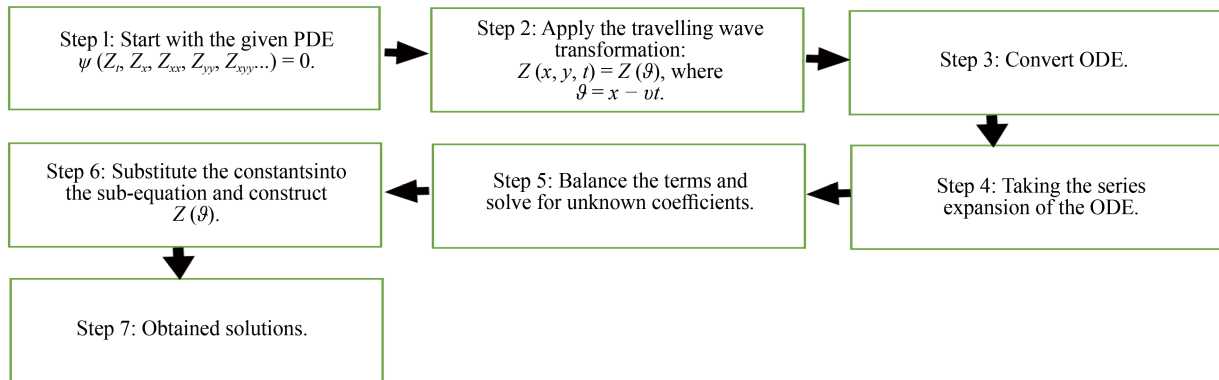


Figure 1. Flow chart 01: The flow chart of the $\frac{AG'}{GE}$ method

The model of the nonlocal nonlinear KE equation is given by [44]:

$$iU_t + c_1 U_{xx} + c_2 U U^*(-x, t)U + c_3 (U U^*(-x, t))^2 U + i c_4 U (U U^*(-x, t))_x = 0. \quad (8)$$

Where $\zeta(-x, t)$ is a complex function of real variables, and the dynamics of optical solitons in birefringent fiber for the nonlocal KE model is shown in Eq. (8). The group velocity c_1 is the dispersion coefficient, and the focusing and defocusing values of cubic and quartic nonlinearities are c_2 and $c_3 = \pm$. c_4 illustrates the Raman scattering self-frequency shifting with focusing and defocusing instances. We employ the $\frac{AG'}{GE}$ method for developing the exact solution of Eq. (8). However, converting the NPDE into an ordinary differential equation of Eq. (8) is our priority. Considering

$$U(x, t) = q(\vartheta) e^{i(\alpha x - \omega t)}, \quad \vartheta = x - vt. \quad (9)$$

Here, v is the wave's speed, α is its wave number, and ω is its angular velocity.

Here,

$$U_t = -(v q_{\vartheta} + i \omega q) e^{i(\alpha x - \omega t)}; \quad (10)$$

$$U_x = (q_{\vartheta} + i \alpha q) e^{i(\alpha x - \omega t)}; \quad (11)$$

$$U_{xx} = (q_{\vartheta\vartheta} + 2i \alpha q_{\vartheta} - \alpha^2 q) e^{i(\alpha x - \omega t)}; \quad (12)$$

$$(U U^*(-x, t))U = q^3 e^{i(3\alpha x - \omega t)}; \quad (13)$$

$$(UU^*(-x, t))^2 U = q^5 e^{i(5\alpha x - \omega t)}; \quad (14)$$

$$(UU^*(-x, t))_x U = (2i\alpha q^3 + 2q^2 q_\vartheta) e^{i(3\alpha x - \omega t)}. \quad (15)$$

Substituting the values of Eqs. (10) to (15) into Eq. (8), we obtain

$$\begin{aligned} & (\omega q - i\nu q_\vartheta) e^{i(\alpha x - \omega t)} + c_1 (q_\vartheta \vartheta + 2i\alpha q - \alpha^2 q) e^{i(\alpha x - \omega t)} + c_2 q^3 e^{i(3\alpha x - \omega t)} + c_3 q^5 e^{i(5\alpha x - \omega t)} + \\ & c_4 (-2\alpha q^3 + 2iq^2 q_\vartheta) e^{i(3\alpha x - \omega t)} = 0. \end{aligned} \quad (16)$$

The exponentials $e^{i(\alpha x - \omega t)}$, $e^{i(3\alpha x - \omega t)}$, and $e^{i(5\alpha x - \omega t)}$ are linearly independent functions, because they oscillate with different wavenumbers. For an identity to hold for all x, t the coefficients multiplying each *distinct* exponential must be zero independently. Therefore, the only way for the sum to vanish identically for all x, t is if the coefficients of each exponential vanish separately.

Therefore,

$$(\omega q - i\nu q_\vartheta) + c_1 (q_\vartheta \vartheta + 2i\alpha q - \alpha^2 q) + c_2 q^3 + c_3 q^5 + c_4 (-2\alpha q^3 + 2iq^2 q_\vartheta) = 0. \quad (17)$$

Equating real and imaginary parts, we have

$$\omega q + c_1 (q_\vartheta \vartheta - \alpha^2 q) + (c_2 - 2c_4 \alpha) q^3 + c_3 q^5 = 0. \quad (18)$$

$$-\nu q_\vartheta + 2c_1 \alpha q_\vartheta + 2c_4 q_\vartheta q^2 = 0. \quad (19)$$

Simplifying Eq. (19) and then integrating, we have

$$-\nu q + 2c_1 \alpha q + \frac{2}{3} c_4 q^3 = 0. \quad (20)$$

In Eq. (20), the integration constant is set to zero. In the 2nd step, $q(\vartheta)$ can be expressed in a series form of the method

$$q(\vartheta) = \sum_{-N}^N K_i S^i. \quad (21)$$

Balancing the highest derivative and nonlinear terms in Eq. (18) yields the balance number $N = \frac{1}{2}$. Hence, substitute $q(\vartheta) = q_1(\vartheta)^{\frac{1}{2}}$ in Eq. (18) and Eq. (20), where $q_1(\vartheta)$ is a new function of ϑ . Eq. (18) and Eq. (20) become

$$\omega q_1 + c_1 \left(\frac{1}{2} q_1'' q_1 - \frac{1}{4} q_1'^2 - \alpha^2 q_1^2 \right) + \left(c_2 - 2c_4 \left(\alpha + \frac{1}{3} \right) \right) q_1^3 + c_3 q_1^4 = 0, \quad (22)$$

$$-v q_1 + 2c_1 \alpha q_1 = 0. \quad (23)$$

Using the principal balance method in Eq. (22) yields the balance number $N = 1$. Accordingly, we obtain the solutions of Eqs. (22) and (23) as follows:

$$q_1(\vartheta) = K_{-1} S^{-1} + K_0 S^0 + K_1 S^1. \quad (24)$$

Here, K_{-1} , K_0 and K_1 are arbitrary constants to be determined. Substitute Eq. (24) into Eqs. (22) and (23).

Applying three cases, we obtained fifteen distinct exact solutions of the nonlocal nonlinear Kundu-Eckhaus equation. A detailed numerical simulation was conducted to determine the effects of parameters on several types of soliton solutions. At the same time, the physical interpretation of the bright, dark, periodic bright, and singular soliton solutions has been extensively explained. Moreover, we analyzed a great deal of MI to predict the formation of localized wave patterns. The efficiency and versatility of the $\frac{AG'}{GE}$ method for complex nonlinear PDEs are examined in this work.

4. Results

Case I:

$$\alpha = \frac{3c_2 - 2c_4}{6c_4}; \lambda = 2(\pm \mu); \mu = \mu; K_0 = 0; K_{-1} = 0;$$

$$\omega = \frac{c_1 c_4}{4 \left(\pm \frac{\sqrt{9c_1 c_2^2 - 12c_1 c_2 c_4 - 32c_1 c_4^2}}{36c_3} \right)};$$

$$K_1 = \pm \frac{\sqrt{9c_1 c_2^2 - 12c_1 c_2 c_4 - 32c_1 c_4^2}}{c_4}.$$

Substituting Case I into Eq. (24), we obtain:

$$U_{11}(x, t) = \left[\pm \frac{\sqrt{9c_1 c_2^2 - 12c_1 c_2 c_4 - 32c_1 c_4^2}}{c_4} \left[\sqrt{\frac{\lambda^2 - 4\mu}{4}} \tanh \left(\sqrt{\frac{\lambda^2 - 4\mu}{4}} (x - vt) \right) \right] \right]^{\frac{1}{2}} e^{i(\alpha x - \omega t)}; \quad (25)$$

$$U_{12}(x, t) = \left[\frac{\sqrt{9c_1 c_2^2 - 12c_1 c_2 c_4 - 32c_1 c_4^2}}{c_4} \left[\sqrt{\frac{\lambda^2 - 4\mu}{4}} \coth \left(\sqrt{\frac{\lambda^2 - 4\mu}{4}} (x - vt) \right) \right] \right]^{\frac{1}{2}} e^{i(\alpha x - \omega t)}; \quad (26)$$

$$U_{13}(x, t) = \left[\frac{\sqrt{9c_1c_2^2 - 12c_1c_2c_4 - 32c_1c_4^2}}{c_4} \left[\frac{1}{(x - vt)} \right] \right]^{\frac{1}{2}} e^{i(\alpha x - \omega t)}; \quad (27)$$

$$U_{14}(x, t) = \left[\frac{\sqrt{9c_1c_2^2 - 12c_1c_2c_4 - 32c_1c_4^2}}{c_4} \left[-\sqrt{-\frac{\lambda^2 - 4\mu}{4}} \tan \left(\sqrt{-\frac{\lambda^2 - 4\mu}{4}} \right) (x - vt) \right] \right]^{\frac{1}{2}} e^{i(\alpha x - \omega t)}; \quad (28)$$

$$U_{15}(x, t) = \left[\frac{\sqrt{9c_1c_2^2 - 12c_1c_2c_4 - 32c_1c_4^2}}{c_4} \left[-\sqrt{-\frac{\lambda^2 - 4\mu}{4}} \cot \left(\sqrt{-\frac{\lambda^2 - 4\mu}{4}} \right) (x - vt) \right] \right]^{\frac{1}{2}} e^{i(\alpha x - \omega t)}. \quad (29)$$

Case II:

$$\alpha = \frac{3c_2 - 2c_4}{6c_4}; m = \pm \sqrt{\frac{9c_1c_2^2 - 12c_1c_2c_4 - 32c_1c_4^2}{c_4}}; \mu = \mu;$$

$$\lambda = \frac{3 \left(\pm \sqrt{\frac{324\mu c_1c_4^2 + 864c_1c_2^3c_4 + 432\mu c_1c_2^2c_4^2 - 1344\mu c_1c_2c_4^3 + 512\mu c_1c_4^4 + 1296mc_4^3c_3}{81c_1c_2^2 - 108c_1c_2c_4 - 288c_1c_4^2}} \right)}{8c_2 - 2c_4};$$

$$\omega = \frac{(9c_2^2 - 12c_2c_4 - 32c_4^2) c_1c_4}{4(9c_2^2 - 12c_2c_4 + 4c_4^2) \left(\pm \frac{\sqrt{9c_1c_2^2 - 12c_1c_2c_4 - 32c_1c_4^2}}{36c_3} \right)};$$

$$K_0 = 0; K_{-1} = 0; K_1 = \pm \frac{\sqrt{\frac{9c_1c_2^2 - 12c_1c_2c_4 - 32c_1c_4^2}{36c_3}}}{c_4}.$$

Substituting Case II into Eq. (24), we obtain:

$$U_{21}(x, t) = \left[\frac{\sqrt{\frac{9c_1c_2^2 - 12c_1c_2c_4 - 32c_1c_4^2}{36c_3}}}{c_4} \left[\sqrt{\frac{\lambda^2 - 4\mu}{4}} \tanh \left(\sqrt{\frac{\lambda^2 - 4\mu}{4}} \right) (x - vt) \right] \right]^{\frac{1}{2}} e^{i(\alpha x - \omega t)}; \quad (30)$$

$$U_{22}(x, t) = \left[\frac{\sqrt{\frac{9c_1c_2^2 - 12c_1c_2c_4 - 32c_1c_4^2}{36c_3}}}{c_4} \left[\sqrt{\frac{\lambda^2 - 4\mu}{4}} \coth \left(\sqrt{\frac{\lambda^2 - 4\mu}{4}} (x - vt) \right) \right] \right]^{\frac{1}{2}} e^{i(\alpha x - \omega t)}; \quad (31)$$

$$U_{23}(x, t) = \left[\frac{\sqrt{\frac{9c_1c_2^2 - 12c_1c_2c_4 - 32c_1c_4^2}{36c_3}}}{c_4} \left[\frac{1}{(x - vt)} \right] \right]^{\frac{1}{2}} e^{i(\alpha x - \omega t)}; \quad (32)$$

$$U_{24}(x, t) = \left[\frac{\sqrt{\frac{9c_1c_2^2 - 12c_1c_2c_4 - 32c_1c_4^2}{36c_3}}}{c_4} \left[-\sqrt{-\frac{\lambda^2 - 4\mu}{4}} \tan \left(\sqrt{-\frac{\lambda^2 - 4\mu}{4}} (x - vt) \right) \right] \right]^{\frac{1}{2}} e^{i(\alpha x - \omega t)}; \quad (33)$$

$$U_{25}(x, t) = \left[\frac{\sqrt{\frac{9c_1c_2^2 - 12c_1c_2c_4 - 32c_1c_4^2}{36c_3}}}{c_4} \left[\sqrt{-\frac{\lambda^2 - 4\mu}{4}} \cot \left(\sqrt{-\frac{\lambda^2 - 4\mu}{4}} (x - vt) \right) \right] \right]^{\frac{1}{2}} e^{i(\alpha x - \omega t)}. \quad (34)$$

Case III:

$$\alpha = \frac{3c_2 - 2c_4}{6c_4}; m = \pm \sqrt{\frac{9c_1c_2^2 - 12c_1c_2c_4 - 32c_1c_4^2}{c_4}}; K_{-1} = \frac{9c_4^2}{4(9c_2^2 - 12c_2c_4 + 4c_4^2)}, \mu = \mu;$$

$$\lambda = \frac{3 \left(\pm \sqrt{\frac{324\mu c_1c_4^2 + 864c_1c_2^3c_4 + 432\mu c_1c_2^2c_4^2 - 1344\mu c_1c_2c_4^3 + 512\mu c_1c_4^4 + 1296mc_4^3c_3}{81c_1c_2^2 - 108c_1c_2c_4 - 288c_1c_4^2}} \right)}{8c_2 - 2c_4};$$

$$\omega = \frac{(9c_2^2 - 12c_2c_4 - 32c_4^2) c_1c_4}{4(9c_2^2 - 12c_2c_4 + 4c_4^2) \left[\pm \frac{\sqrt{9c_1c_2^2 - 12c_1c_2c_4 - 32c_1c_4^2}}{36c_3} \right]};$$

$$K_0 = 0; K_1 = \pm \frac{\sqrt{\frac{9c_1c_2^2 - 12c_1c_2c_4 - 32c_1c_4^2}{36c_3}}}{c_4}.$$

Substituting Case III into Eq. (24), we obtain:

$$U_{31}(x, t) = \left[\frac{9c_4^2}{4(9c_2^2 - 12c_2c_4 + 4c_4^2)} \left[\sqrt{\frac{\lambda^2 - 4\mu}{4}} \tanh \left(\sqrt{\frac{\lambda^2 - 4\mu}{4}} (x - vt) \right) \right]^{-1} \right. \\ \left. \pm \frac{\sqrt{\frac{9c_1c_2^2 - 12c_1c_2c_4 - 32c_1c_4^2}{36c_3}}}{c_4} \left[\sqrt{\frac{\lambda^2 - 4\mu}{4}} \tanh \left(\sqrt{\frac{\lambda^2 - 4\mu}{4}} (x - vt) \right) \right] \right]^{\frac{1}{2}} e^{i(\alpha x - \omega t)}; \quad (35)$$

$$U_{32}(x, t) = \left[\frac{9c_4^2}{4(9c_2^2 - 12c_2c_4 + 4c_4^2)} \left[\sqrt{\frac{\lambda^2 - 4\mu}{4}} \coth \left(\sqrt{\frac{\lambda^2 - 4\mu}{4}} (x - vt) \right) \right]^{-1} \right. \\ \left. \pm \frac{\sqrt{\frac{9c_1c_2^2 - 12c_1c_2c_4 - 32c_1c_4^2}{36c_3}}}{c_4} \left[\sqrt{\frac{\lambda^2 - 4\mu}{4}} \coth \left(\sqrt{\frac{\lambda^2 - 4\mu}{4}} (x - vt) \right) \right] \right]^{\frac{1}{2}} e^{i(\alpha x - \omega t)}; \quad (36)$$

$$U_{33}(x, t) = \left[\frac{9c_4^2}{4(9c_2^2 - 12c_2c_4 + 4c_4^2)} \left[\frac{1}{(x - vt)} \right]^{-1} \right. \\ \left. \pm \frac{\sqrt{\frac{9c_1c_2^2 - 12c_1c_2c_4 - 32c_1c_4^2}{36c_3}}}{c_4} [ck1(x - vt)] \right]^{\frac{1}{2}} e^{i(\alpha x - \omega t)}; \quad (37)$$

$$U_{34}(x, t) = \left[\frac{9c_4^2}{4(9c_2^2 - 12c_2c_4 + 4c_4^2)} \left[-\sqrt{-\frac{\lambda^2 - 4\mu}{4}} \tan \left(\sqrt{-\frac{\lambda^2 - 4\mu}{4}} (x - vt) \right) \right]^{-1} \right. \\ \left. \pm \frac{\sqrt{\frac{9c_1c_2^2 - 12c_1c_2c_4 - 32c_1c_4^2}{36c_3}}}{c_4} \left[-\sqrt{-\frac{\lambda^2 - 4\mu}{4}} \tan \left(\sqrt{-\frac{\lambda^2 - 4\mu}{4}} (x - vt) \right) \right] \right]^{\frac{1}{2}} e^{i(\alpha x - \omega t)}; \quad (38)$$

$$U_{35}(x, t) = \left[\frac{9c_4^2}{4(9c_2^2 - 12c_2c_4 + 4c_4^2)} \left[\sqrt{-\frac{\lambda^2 - 4\mu}{4}} \cot \left(\sqrt{-\frac{\lambda^2 - 4\mu}{4}} (x - vt) \right) \right]^{-1} \right. \\ \left. \pm \frac{\sqrt{\frac{9c_1c_2^2 - 12c_1c_2c_4 - 32c_1c_4^2}{36c_3}}}{c_4} \left[\sqrt{-\frac{\lambda^2 - 4\mu}{4}} \cot \left(\sqrt{-\frac{\lambda^2 - 4\mu}{4}} (x - vt) \right) \right]^{\frac{1}{2}} \right] e^{i(\alpha x - \omega t)}. \quad (39)$$

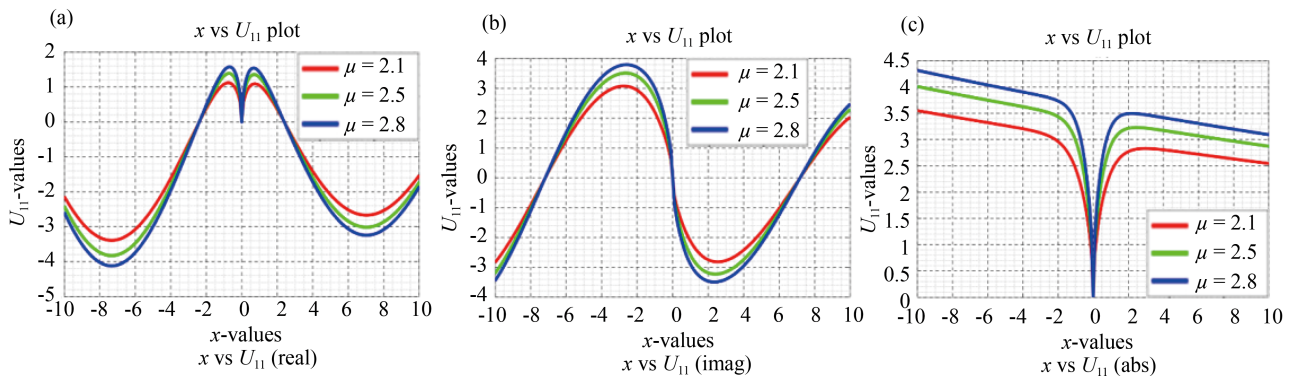
5. Discussion

To elucidate the fundamental physical phenomena of nonlinear sciences such as plasma physics, optics, soliton waves, computer networking, acoustics, and heat transfer, the exact soliton solutions of NLPDEs are playing a crucial role. Numerous researchers have employed various methods to understand the characteristics of optical waves utilizing solutions obtained from different NLPDEs. We employed the $\left(\frac{AG'}{GE}\right)$ method to this article to find our desired optical solutions for the nonlocal KE equation. We obtained fifteen distinct solutions for three cases. For a better understanding of optical properties in a birefringent medium, we plotted 2D, 3D, and contour plots for five representative solutions. After plotting these solutions, we got periodic bright and dark solitons, singular solitons, and bright and dark solitons. In this section, we present 2D plots, contour plots, and finally 3D plots of these five solutions.

5.1 2D graphical representations for different values of μ , t and x

Providing the effect of parameters μ , t and x of the equation U_{11} drawn Figures 2a-i in this subsection show real, imaginary, and absolute values. In Figure 2a-c, we presented 2D [(a) Real, (b) Imaginary, (c) Absolute] plots of $U_{11}(x, t)$ varying the parameter μ marked in figure and shown in red, green, and blue color respectively, where other constants are $c_1 = 1.1$, $c_2 = 0.01$, $c_3 = 0.01$, $c_4 = 1.0$, $\vartheta = 1.5$ within $-10 \leq x \leq 10$ and $-10 \leq t \leq 10$. Figures 2D, 2f, and 2h show the real, imaginary, and absolute values versus parameters colored in red, green, and blue respectively. Figures 2e, 2g, and 2i displayed t versus U_{11} of real, imaginary and absolute values for $x = 1$, $x = 2$ and $x = 3$ in red, green, and blue, respectively. From this solution, we received periodic bright and dark solitons following parameters $\alpha = -0.3283$, $K_0 = 0$, $K_{-1} = 0$, $K_1 = -5.440i$, $\lambda = 4.2$, $\omega = -0.0167i$ for the case I. Periodic bright solitons describe localized optical pulses or plasma wave packets that self-focus, while dark solitons correspond to an intensity “hole” in a continuous-wave background. Bright solitons are crucial for long-distance optical communication since they can propagate without distortion. The existence of bright solitons in the nonlocal PT-symmetric KE model suggests ways to design stable energy-localized modes in birefringent fibers and PT waveguides, while dark solitons are important for information encoding and switching in optical fibers, since they provide stable intensity dips that are less sensitive to perturbations. Their stability analysis in the nonlocal KE framework shows how defocusing nonlinearities affect wave robustness. From Figure 3a-3c, we demonstrated a 2D [(a) Real, (b) Imaginary, (c) Absolute] plot of $U_{12}(x, t)$ varying the parameters μ as shown in the figure, colored in red, green, and blue respectively, while the other values are fixed as $c_1 = 1.1$, $c_2 = 0.01$, $c_3 = 0.01$, $c_4 = 0.5$, $\vartheta = 1.5$ within $-10 \leq x \leq 10$ and $-10 \leq t \leq 10$. Figures 3d, 3f, 3h are displayed x versus U_{12} of real, imaginary and absolute values respectively for $t = 1$, $t = 1.5$, $t = 2$ while colors are fixed as red, green, and blue respectively and the Figures 3e, 3g, 3i represent t versus U_{12} of real, imaginary and absolute values for $x = 1$, $x = 1.5$ and $x = 2$ colored in red, green and blue respectively. Observing the solution, we obtained bright and singular solitons following the parameters $\alpha = -0.3233$, $K_0 = 0$, $K_{-1} = 0$, $K_1 = -5.9548i$, $\lambda = 3$, $\omega = -0.0166i$ for the case II. Singular solutions highlight the limits of stability in nonlinear wave propagation. These solitons show parameter regimes where physical systems may experience

disastrous collapse, which is essential in laser-plasma interactions and optical filamentation studies. Furthermore, in Figures 4a-4c, we visualized 2D [(a) Real, (b) Imaginary, (c) Absolute] plots of $U_{24}(x, t)$ under parameter μ as shown in the figure, colored in red, green, and blue respectively while other constants are $c_1 = 1.1$, $c_2 = 2.1$, $c_3 = 1.5$, $c_4 = 0.5$, $\vartheta = 1.2$ within $-5 \leq x \leq 5$ and $-5 \leq t \leq 5$. When $t = 1, t = 1.5, t = 2$, in Figure 4d-4h manifested x versus U_{24} of real, imaginary and absolute values and designed in red, green, and blue respectively as well as the Figure 4e-4i are displayed t versus U_{24} of real, imaginary and absolute values for $x = 1, x = 1.5$ and $x = 2$. The solutions are periodic bright and dark, and V-shaped solitons following the parameters $\alpha = 1.7667$, $K_0 = 0$, $K_{-1} = 0$, $K_1 = 1.2472$, $\lambda = 1.0884$, $\omega = 1.1012$ for the case II. Periodic bright solitons describe wave trains and modulational patterns in nonlinear fiber optics, which are precursors to rogue waves or complex wave turbulence while periodic dark solitons describe regularly spaced phase defects on a continuous-wave background. In Figure 5a-5c, we exhibited 2D [(a) Real, (b) Imaginary, (c) Absolute] plots of $U_{32}(x, t)$ regime parameters $\mu = 0.7, \mu = 0.9$ and $\mu = 1.1$, and colored in red, green, and blue respectively, while other parameters are $c_1 = -1.2$, $c_2 = -1.1$, $c_3 = 2.01$, $c_4 = 1.4$, $\vartheta = 1.5$ within $-10 \leq x \leq 10$ and $-10 \leq t \leq 10$. Figures 5d, 5f and 5h reveals x versus U_{32} of real, imaginary and absolute values respectively for $t = 1, t = 1.5, t = 2$ in red, green and blue, whereas the Figures 5e, 5g, and 5i display t versus U_{32} of real, imaginary and absolute values for $x = 1, x = 1.5$, and $x = 2$ respectively. Investigating the solution we obtain multiple bright and dark, and bright solitons to the following parameters $\alpha = -0.7262$, $K_0 = 0$, $K_{-1} = 0.1185$, $K_1 = 0.5312$, $\lambda = -2.5014$, $\omega = 4.3053$ for the case III. Beyond the single bright and dark solitons, the system also admits multiple bright and dark soliton configurations, corresponding to interacting trains of localized pulses. In nonlinear optics, such multi-soliton states represent pulse sequences in fibers; in plasmas, they model successive compressive or rarefactive structures; and in hydrodynamics, they correspond to groups of solitary surface waves. We demonstrates 2D [(a) Real, (b) Imaginary, (c) Absolute] plots in Figure 6a-6c of $U_{35}(x, t)$ the following parameters $\mu = 1.5, \mu = 1.75$ and $\mu = 1.95$ colored in red, green, and blue respectively where other parameters are $c_1 = -0.5$, $c_2 = 0.2$, $c_3 = 0.1$, $c_4 = -0.2$, $\vartheta = 0.75$ within $-5 \leq x \leq 5$ and $-5 \leq t \leq 5$. The Figures 6d-6h show x versus U_{35} of real, imaginary and absolute values respectively for $t = 0.5, t = 1.0, t = 1.5$ in red, green, and blue respectively and the other Figures are 6e-6i represent t versus U_{35} of real, imaginary and absolute values following $x = 0.5, x = 1.0$ and $x = 1.5$ shown in red, green and blue respectively. Analyzing the solution U_{35} , we have periodic bright solitons following the parameters $\alpha = -0.8333$, $K_0 = 0$, $K_{-1} = 0.0900$, $K_1 = -2.3452$, $\lambda = 3.2584i$, $\omega = -0.0844$ for the case III.



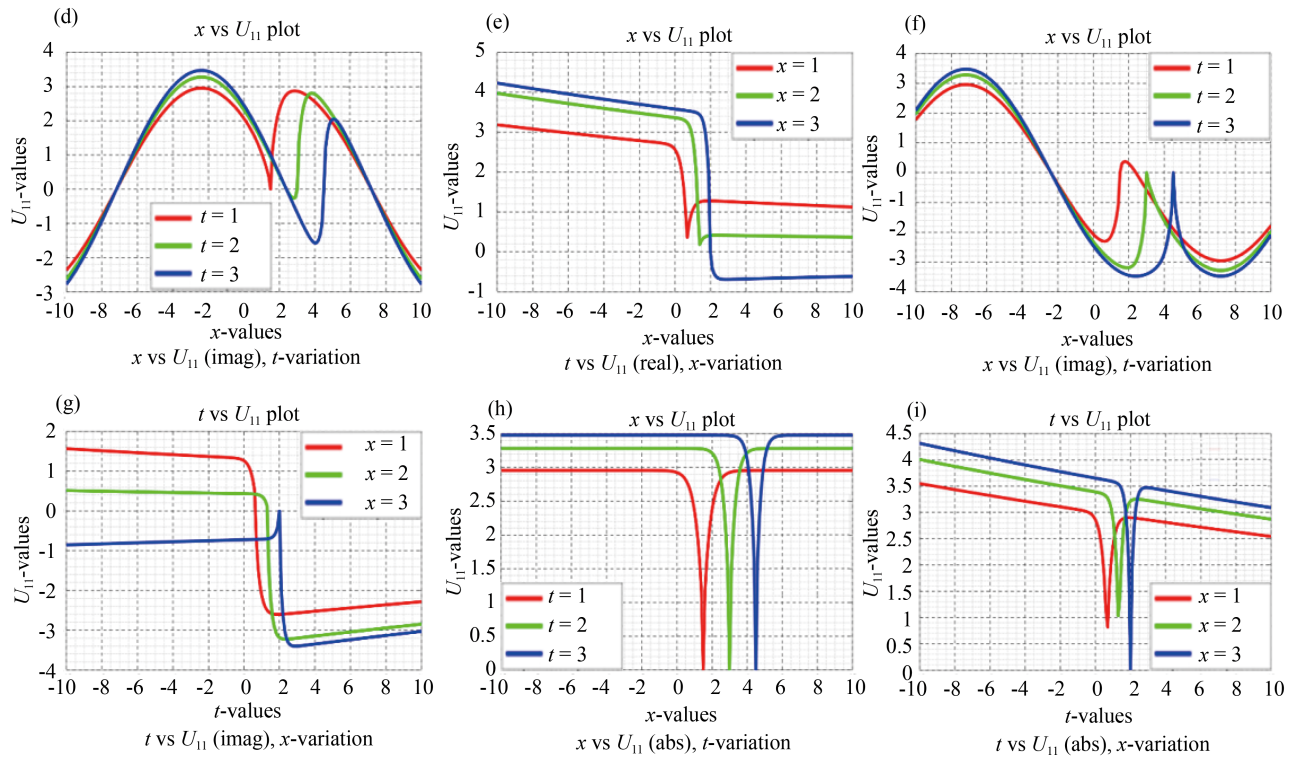
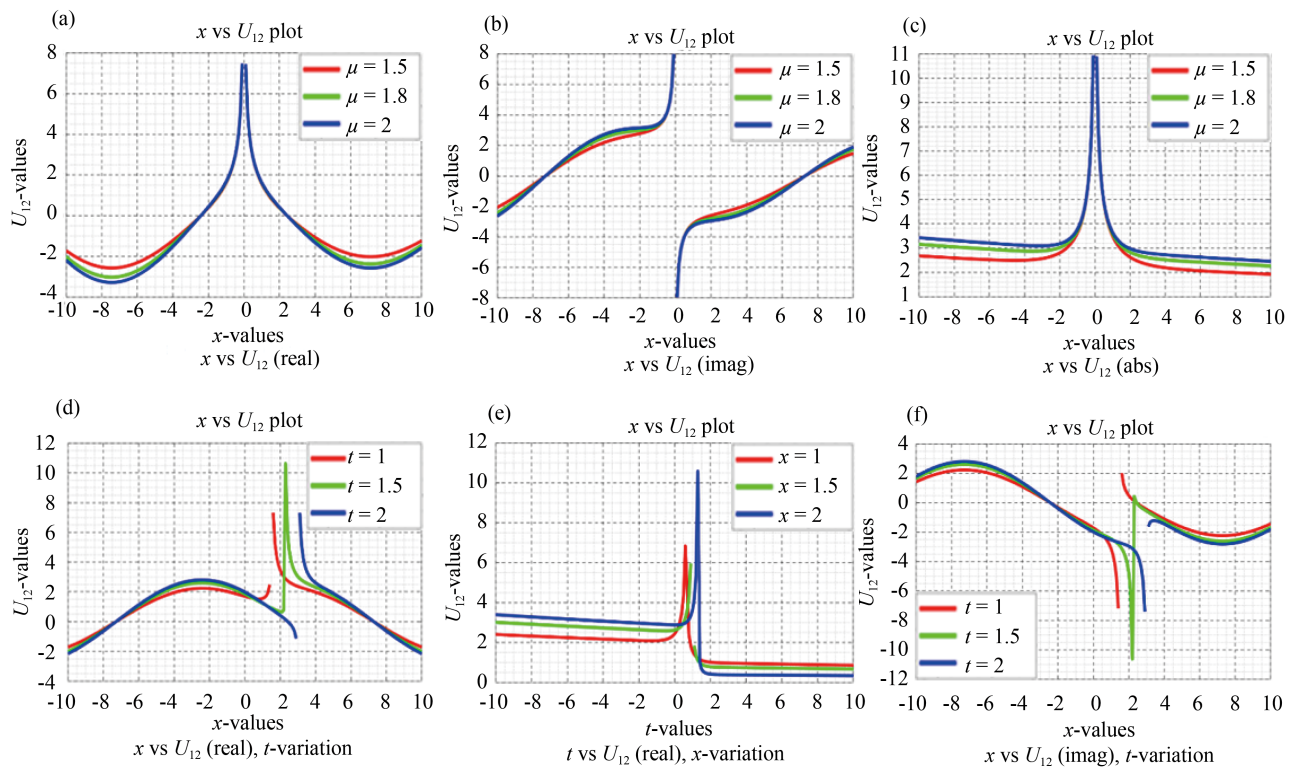


Figure 2. 2D plots of the solution U_{11}



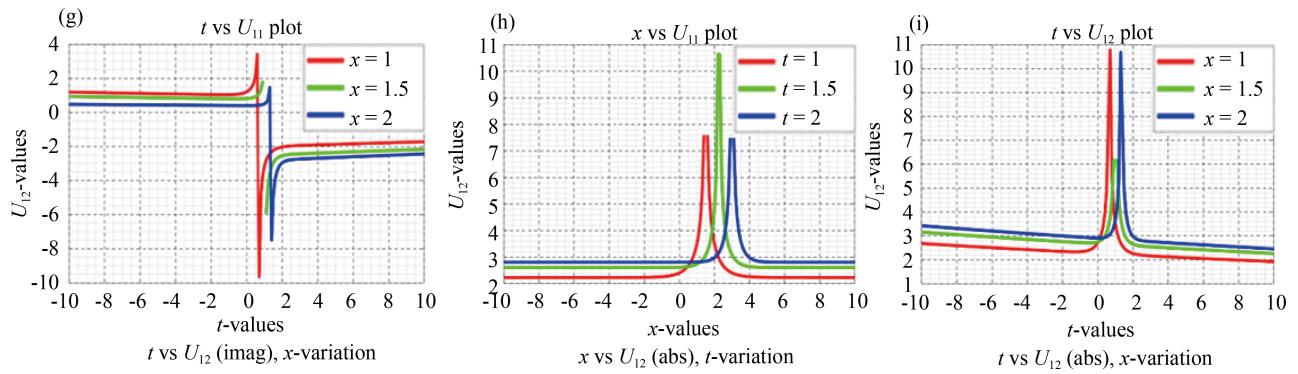


Figure 3. 2D plots of the solution U_{12}

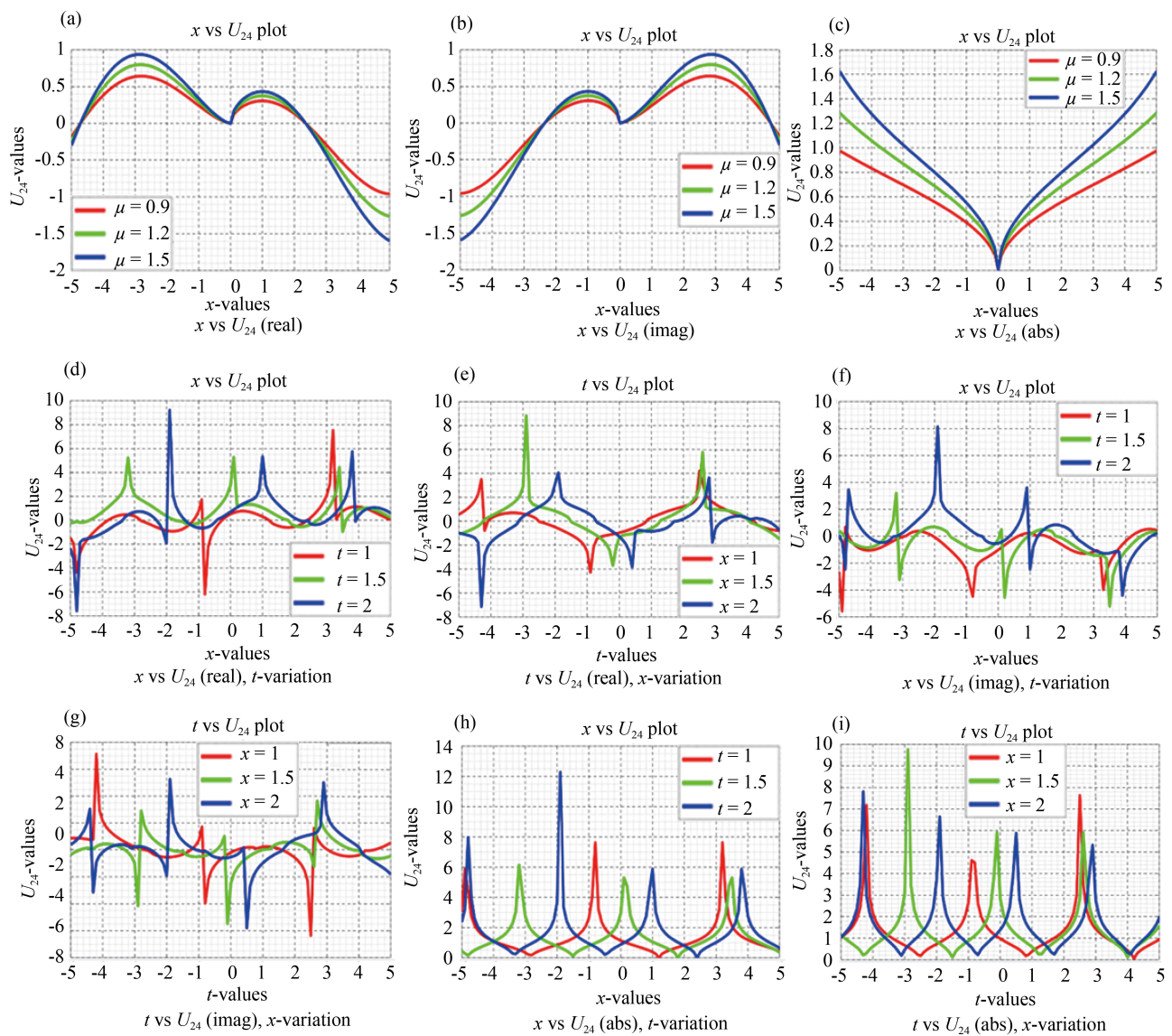


Figure 4. 2D plots of the solution U_{24}

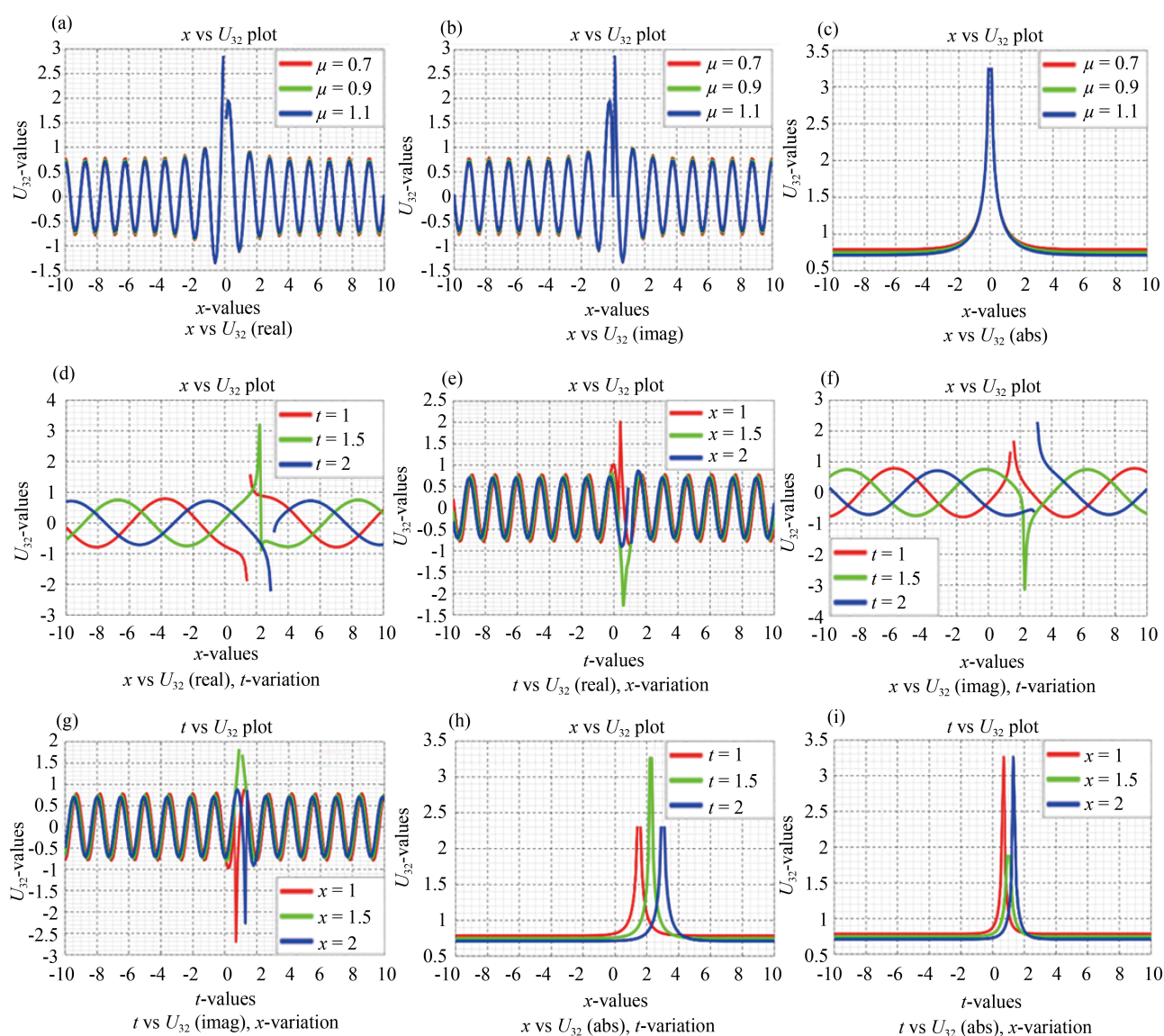
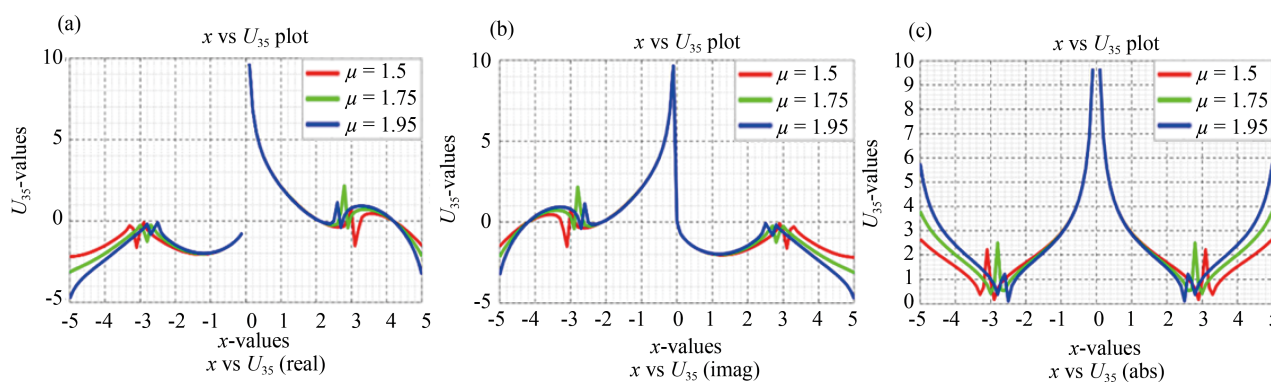


Figure 5. 2D plots of the solution U_{32}



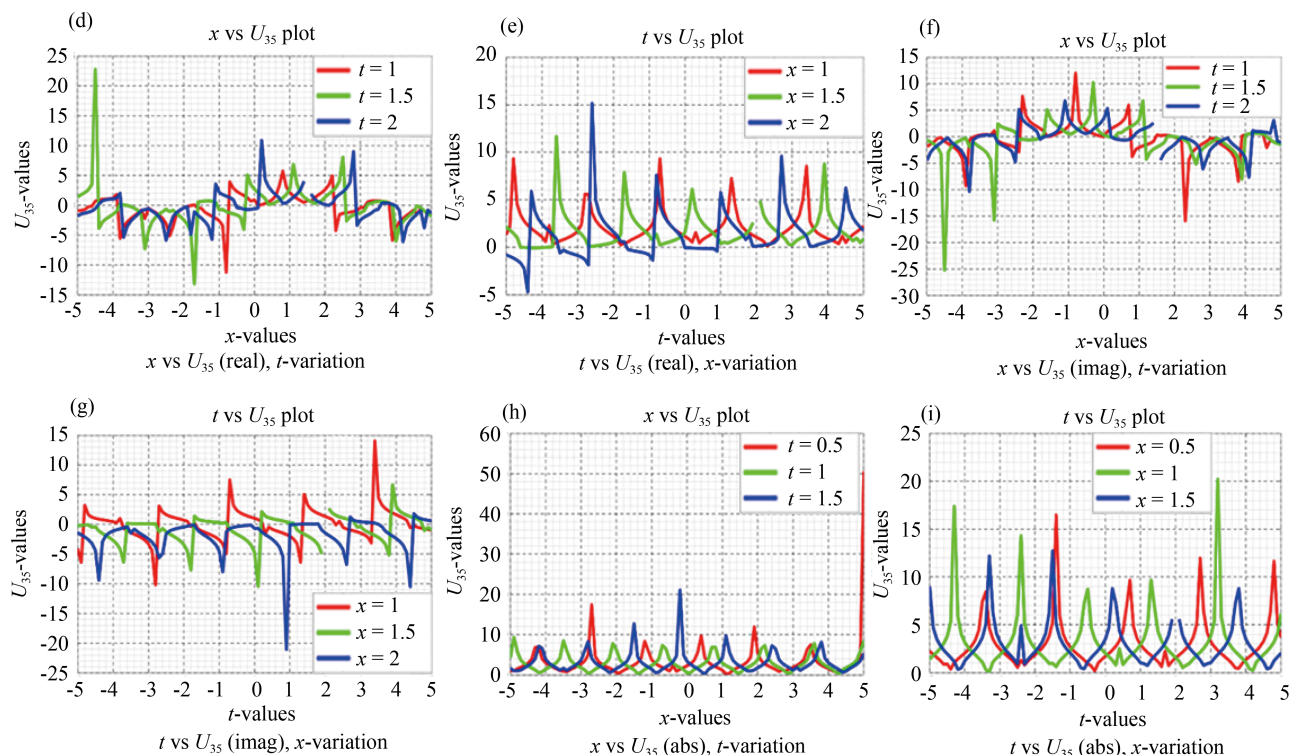


Figure 6. 2D plots of the solution U_{35}

5.2 Graphical representation of contour plots

In this subsection, we exhibit the graphical representation of the solutions of the nonlocal KE equation as contour surfaces. Figure 7a-7c reveals contour [(a) Real, (b) Imaginary, (c) Absolute] plots of periodic bright and dark solitons of $U_{11}(x, t)$ following $\mu = 2.1$, $c_1 = 1.1$, $c_2 = 0.01$, $c_3 = 0.01$, $c_4 = 1.0$, $\vartheta = 1.5$ within $-10 \leq x \leq 10$ and $-10 \leq t \leq 10$, and as well as the other parameters are $\alpha = -0.3283$, $K_0 = 0$, $K_{-1} = 0$, $K_1 = -5.440i$, $\lambda = 4.2$, $\omega = -0.0167i$. In contour plots, it appears as a series of localized peaks repeating in both space and time. When wave pulses propagate, trains of bright optical pulses in nonlinear fibers, cnoidal wave groups in shallow water, or compressive plasma wave trains are generated. In Figure 8a-8c, we demonstrate contour [(a) Real, (b) Imaginary, (c) Absolute] plots of $U_{12}(x, t)$ for $\mu = 1.5$, $c_1 = 1.1$, $c_2 = 0.01$, $c_3 = 0.01$, $c_4 = 0.5$, and $\vartheta = 1.5$ within $-10 \leq x \leq 10$ and $-10 \leq t \leq 10$, and also for the following parameters $\alpha = -0.3233$, $K_0 = 0$, $K_{-1} = 0$, $K_1 = -5.9548i$, $\lambda = 3$, $\omega = -0.0166i$. For this case, bright solitons are localized pulse-type solutions on a zero background, arising when focusing nonlinearity balances dispersion. Dark solitons, by contrast, exist on a finite background and appear as localized intensity dips associated with a phase shift. They are supported by defocusing nonlinearity, describing intensity holes in optical fibers, refraction structures in plasmas, and depressions in hydrodynamic wave trains. Figure 9a-9c represents contour [(a) Real, (b) Imaginary, (c) Absolute] plots of periodic bright and dark solitons for the following constants $\mu = 0.9$, $c_1 = 1.1$, $c_2 = 2.1$, $c_3 = 1.5$, $c_4 = 0.5$, and $\vartheta = 1.2$ within $-5 \leq x \leq 5$ and $-5 \leq t \leq 5$, when others are $\alpha = 1.7667$, $K_0 = 0$, $K_{-1} = 0$, $K_1 = 1.2472$, $\lambda = 1.0884$, $\omega = 1.1012$. We exhibit contour [(a) Real, (b) Imaginary, (c) Absolute] plots in $U_{32}(x, t)$ in Figure 10a-10c as multiple bright and dark solitons using $\mu = 0.7$, where other constants are $c_1 = -1.2$, $c_2 = -1.1$, $c_3 = 2.01$, $c_4 = 1.4$, and $\vartheta = 1.5$ within $-10 \leq x \leq 10$ and $-10 \leq t \leq 10$ and other parameters are $\alpha = -0.7262$, $K_0 = 0$, $K_{-1} = 0.1185$, $K_1 = 0.5312$, $\lambda = -2.5014$, $\omega = 4.3053$. Multi-soliton exhibits multiple localized structures as peaks or dips. It represents successive solitary structures in plasma, or wave groups in hydrodynamics. Figure 11a-11c illustrates contour [(a) Real, (b) Imaginary, (c) Absolute] plots of periodic bright soliton for $U_{35}(x, t)$ followed $\mu = 1.5$, $c_1 = -0.5$, $c_2 = 0.2$,

$c_3 = 0.1$, $c_4 = -0.2$, and $\vartheta = 0.75$ within $-5 \leq x \leq 5$ and $-5 \leq t \leq 5$, where other necessary constants are $\alpha = -0.8333$, $K_0 = 0$, $K_{-1} = 0.0900$, $K_1 = -2.3452$, $\lambda = 3.2584i$, $\omega = -0.0844$.

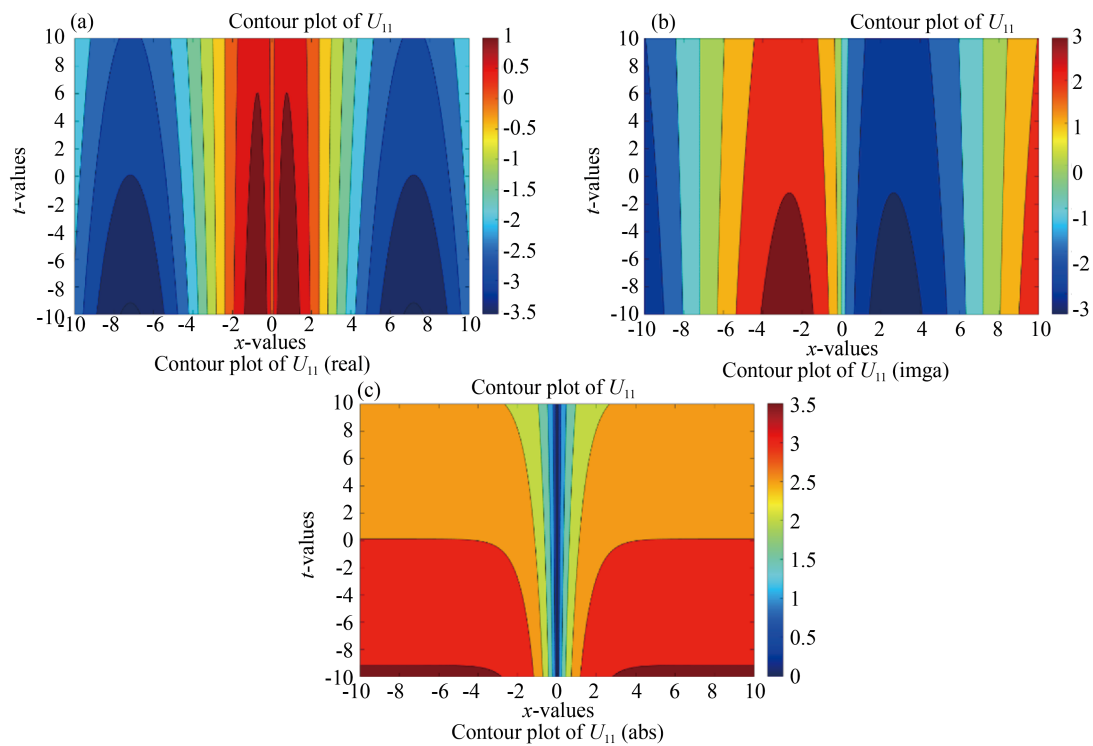
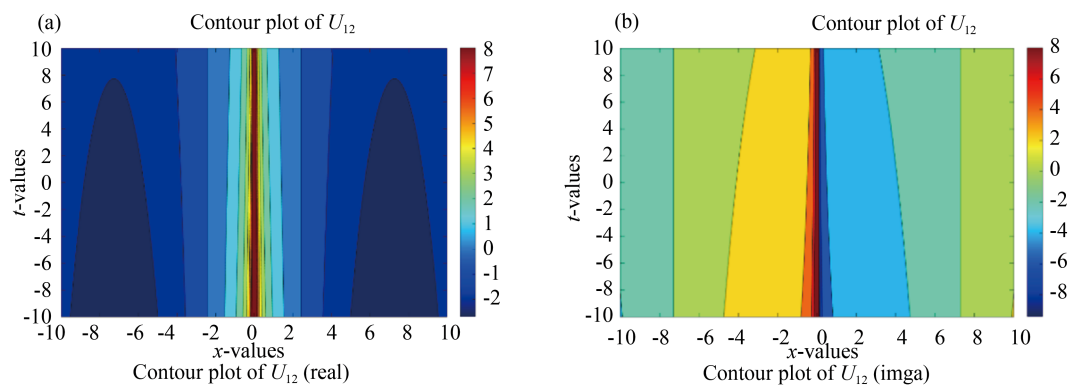


Figure 7. Contour plots of the solution U_{11}



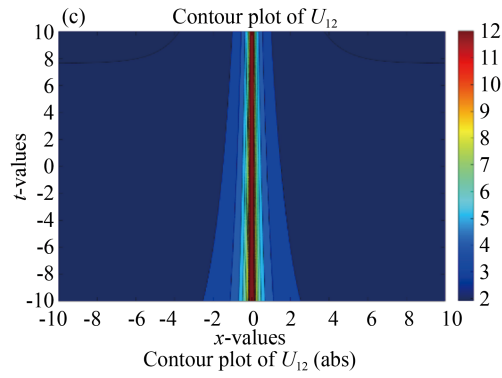


Figure 8. Contour plots of the solution U_{12}

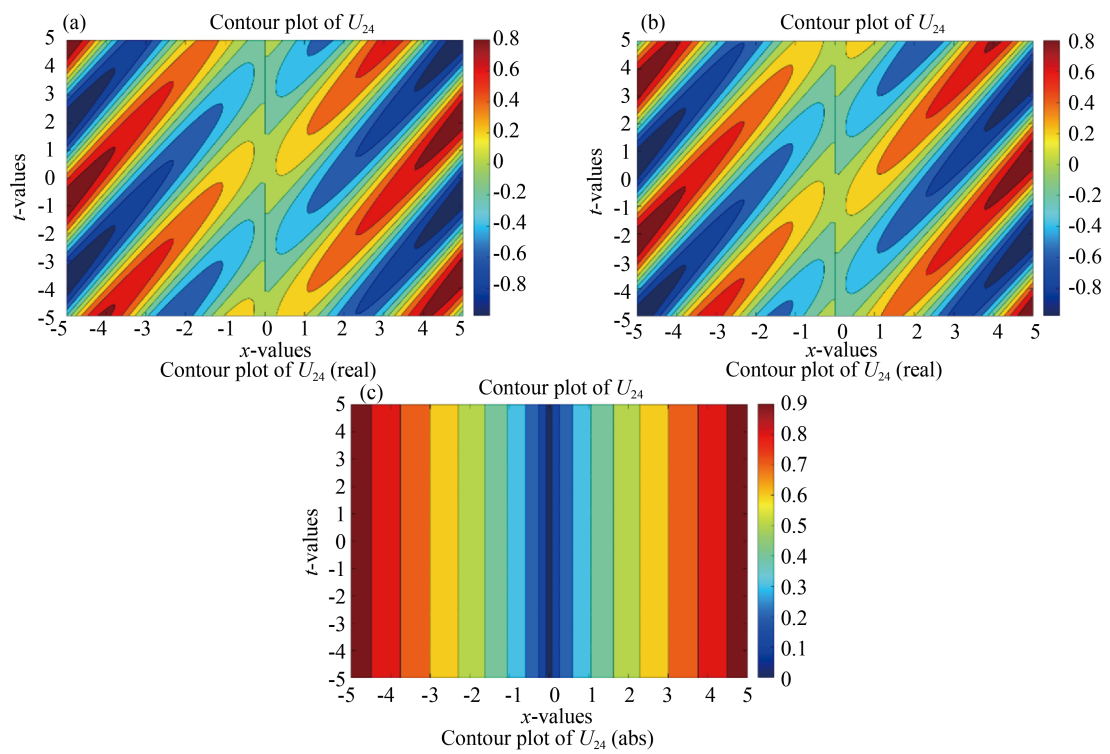


Figure 9. Contour plots of the solution U_{24}

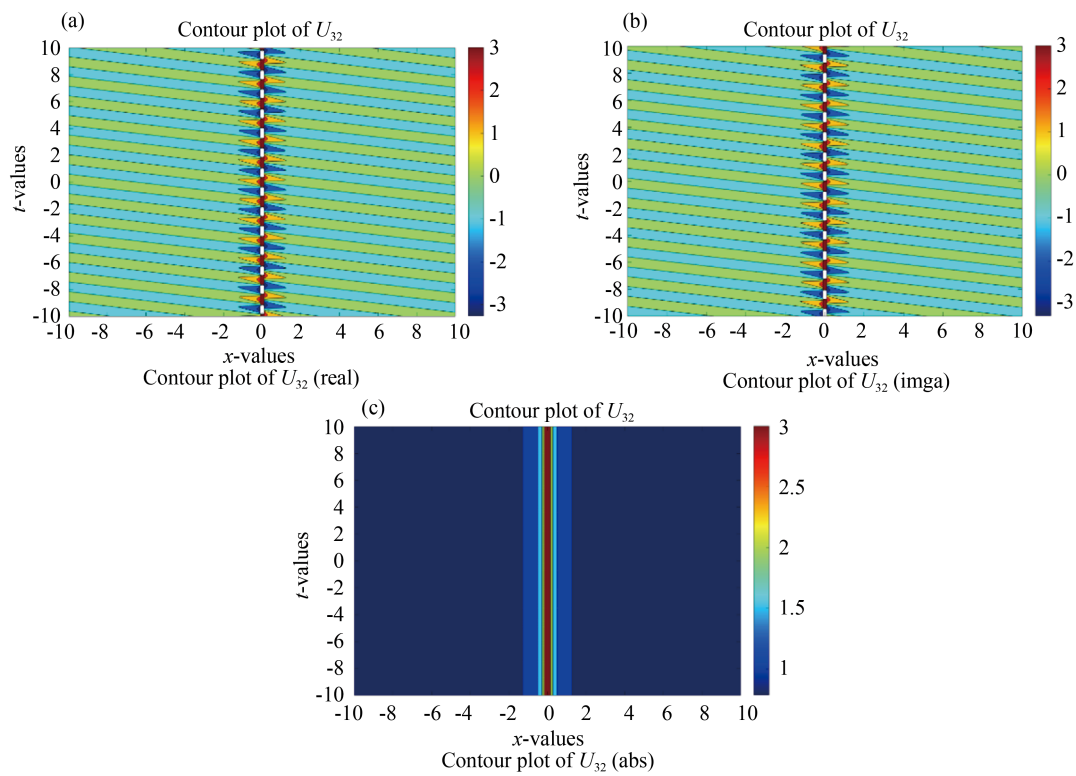


Figure 10. Contour plots of the solution U_{32}

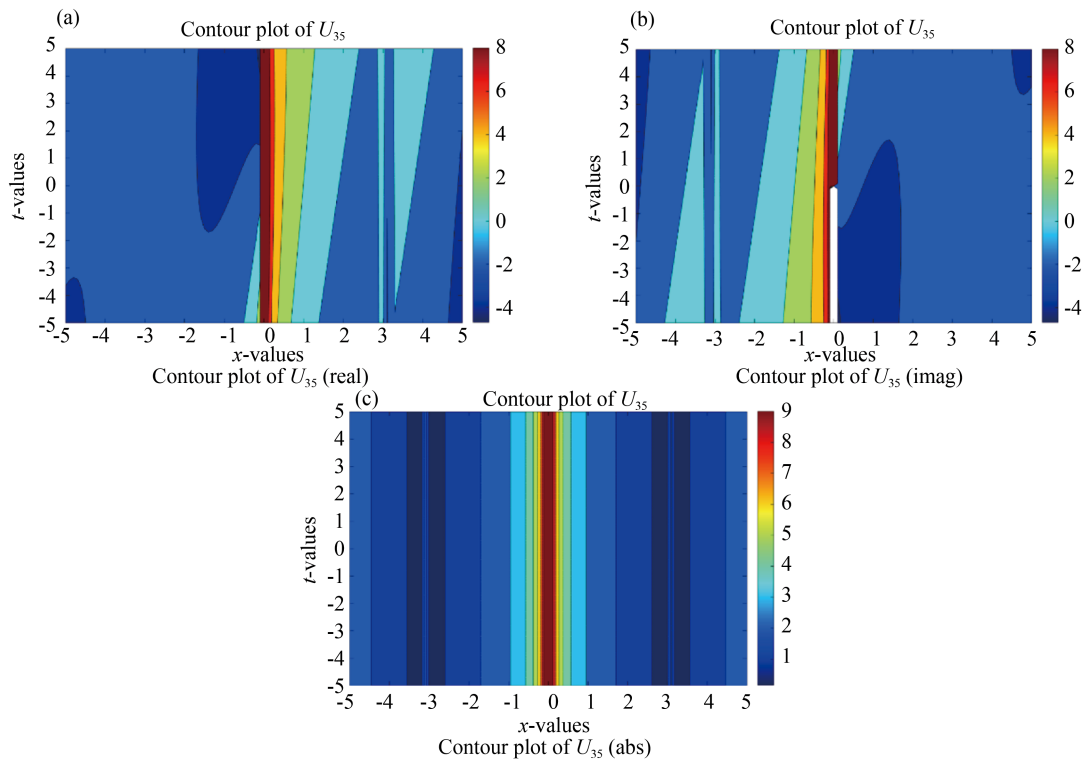


Figure 11. Contour plots of the solution U_{35}

5.3 3D graphical representation

In this subsection, we demonstrated the 3D graphical visualization of the solutions of the nonlocal KE equation as contour surfaces. Figure 12a-12c represents the physical appearance of $U_{11}(x, t)$ [(a) Real, (b) Imaginary, (c) Absolute] in 3D surfaces for $\mu = 2.1$, $c_1 = 1.1$, $c_2 = 0.01$, $c_3 = 0.01$, $c_4 = 1.0$, $\vartheta = 1.5$ within $-10 \leq x \leq 10$ and $-10 \leq t \leq 10$ following $\alpha = -0.3283$, $K_0 = 0$, $K_{-1} = 0$, $K_1 = -5.440i$, $\lambda = 4.2$, $\omega = -0.0167$. The solution offers periodic bright and dark solitons. It illustrates a stable, localized disturbance that travels through space without changing its fundamental shape. In periodic refractive index media, light can form gap solitons, periodic bright structures that are confined due to the bandgap of the medium. These are crucial for all-optical switching, optical memory, logic gates and controlling light in integrated photonic circuits. Figure 13a-13c reveals the performance of $U_{12}(x, t)$ as 3D [(a) Real, (b) Imaginary, (c) Absolute] plots for the parameter $\mu = 1.5$ as well as other constants are $c_1 = 1.1$, $c_2 = 0.01$, $c_3 = 0.01$, $c_4 = 0.5$, $\vartheta = 1.5$ within $-10 \leq x \leq 10$ and $-10 \leq t \leq 10$ offering $\alpha = -0.3233$, $K_0 = 0$, $K_{-1} = 0$, $K_1 = -5.9548i$, $\lambda = 3$, $\omega = -0.0166i$. We got bright and singular solitons of this solution. Bright solitons are the backbone of soliton-based optical communication systems. In optical fibers, dispersion tends to broaden pulses, while the Kerr nonlinearity compresses them. When balanced, bright solitons form pulses that can travel thousands of kilometers without distortion. Singular solitons describe ultra-short, high-intensity pulses where the electric field gradient becomes very large useful for modeling femtosecond laser pulses or filamentation. The Figure 14a-14c demonstrates 3D [(a) Real, (b) Imaginary, (c) Absolute] plots of $U_{24}(x, t)$ for constants $\mu = 0.9$, $c_1 = 1.1$, $c_2 = 2.1$, $c_3 = 1.5$, $c_4 = 0.5$, $\vartheta = 1.2$ within $-5 \leq x \leq 5$ and $-5 \leq t \leq 5$ considering $\alpha = 1.7667$, $K_0 = 0$, $K_{-1} = 0$, $K_1 = 1.2472$, $\lambda = 1.0884$, $\omega = 1.1012$. This solution produces periodic bright and dark, and V-shaped solitons. A periodic dark soliton is a periodic wave in which dips or holes repeat regularly against a continuous-wave background. In ultrafast lasers, dark pulse trains can form and are related to frequency combs equally spaced spectral lines used in precision metrology, optical clocks, and spectroscopy. In electrical lattices or magnetized plasmas with periodic structures, dark soliton trains model modulated voltage or density dispersion, useful for signal processing and energy localization. V-solitons reveal the richness of multi-soliton dynamics in higher dimensions and under resonant conditions. The vertex of the V often corresponds to a region of high amplitude or energy concentration, and useful for applications in laser machine, plasma heating, signal amplification in nonlinear optics. V-solitons can act as nonlinear “AND” gates, and output only when two input solitons arrive in resonance. Figure 15a-15c exhibits 3D [(a) Real, (b) Imaginary, (c) Absolute] plots of $U_{32}(x, t)$ using $\mu = 0.7$, $c_1 = -1.2$, $c_2 = -1.1$, $c_3 = 2.01$, $c_4 = 1.4$, $\vartheta = 1.5$ within $-10 \leq x \leq 10$ and $-10 \leq t \leq 10$ following the parameters $\alpha = -0.7262$, $K_0 = 0$, $K_{-1} = 0.1185$, $K_1 = 0.5312$, $\lambda = -2.5014$, $\omega = 4.3053$. Multiple bright and dark, and bright solitons have been allocated for the solution $U_{32}(x, t)$. Multiple bright and dark solitons are not just “more solitons”, they represent the collective, interactive, and coherent nature of nonlinear wave systems. Multiple bright and dark are crucial for information encoding in optical communication in optical communications, and quantum state preservation in matter-wave interferometry. Figure 16a-16c reveals 3D [(a) Real, (b) Imaginary, (c) Absolute] plots of $U_{35}(x, t)$ assigning $\mu = 1.5$, $c_1 = -0.5$, $c_2 = 0.2$, $c_3 = 0.1$, $c_4 = -0.2$, $\vartheta = 0.75$ within $-5 \leq x \leq 5$ and $-5 \leq t \leq 5$ using $\alpha = -0.8333$, $K_0 = 0$, $K_{-1} = 0.0900$, $K_1 = -2.3452$, $\lambda = 3.2584i$, $\omega = -0.0844$. These plots represent multi-soliton structures specifically multi-bright solitons. The most important feature is the coexistence of two solitons. Multiple bright solitons can carry independent bits of information without dispersion-induced distortion.

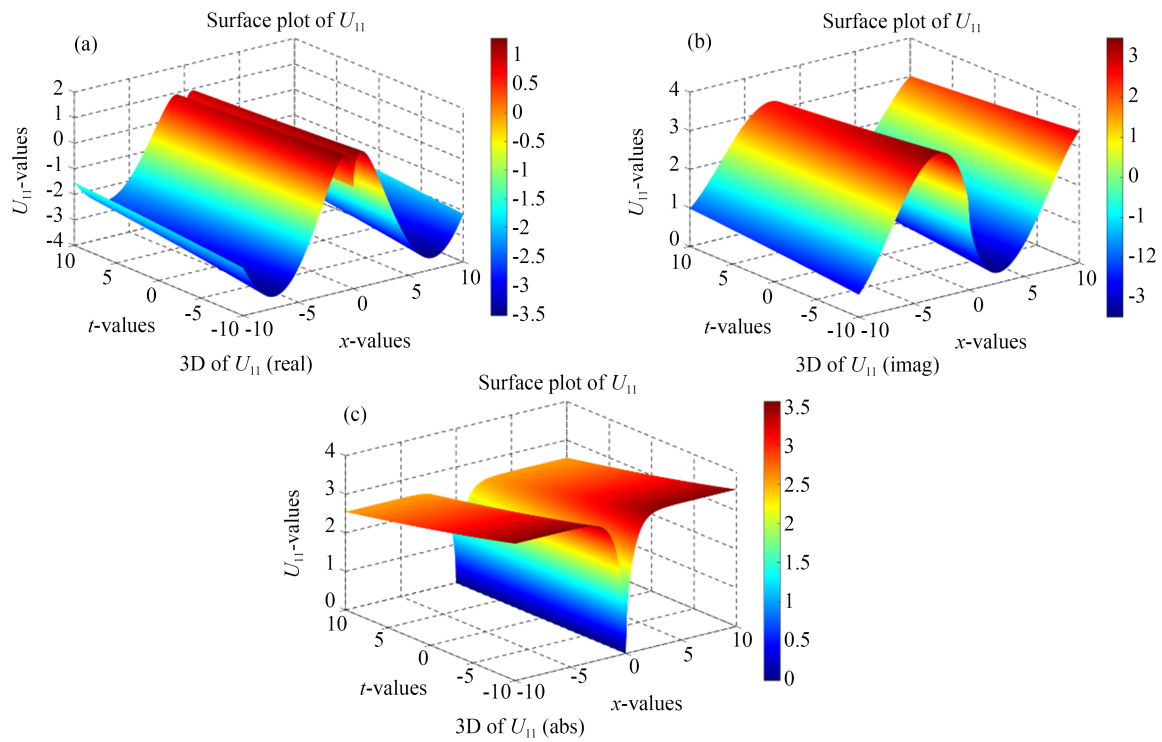


Figure 12. 3D plots of the solution U_{11}

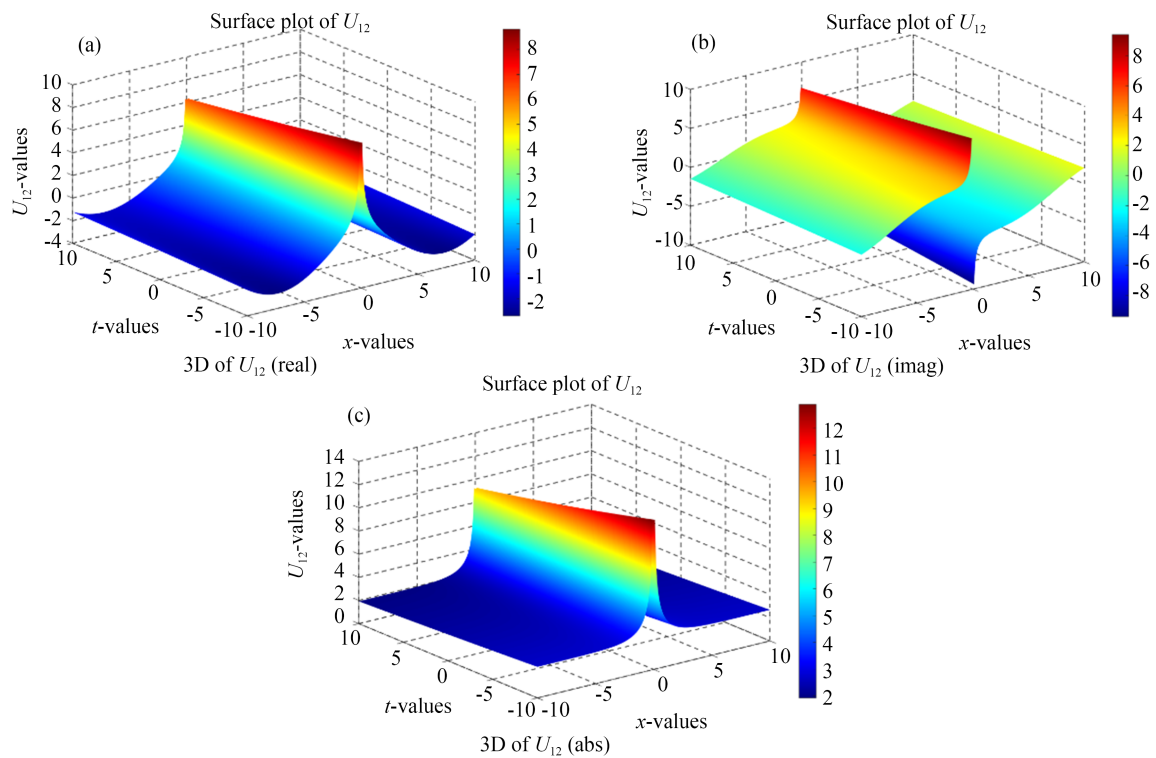


Figure 13. 3D plots of the solution U_{12}

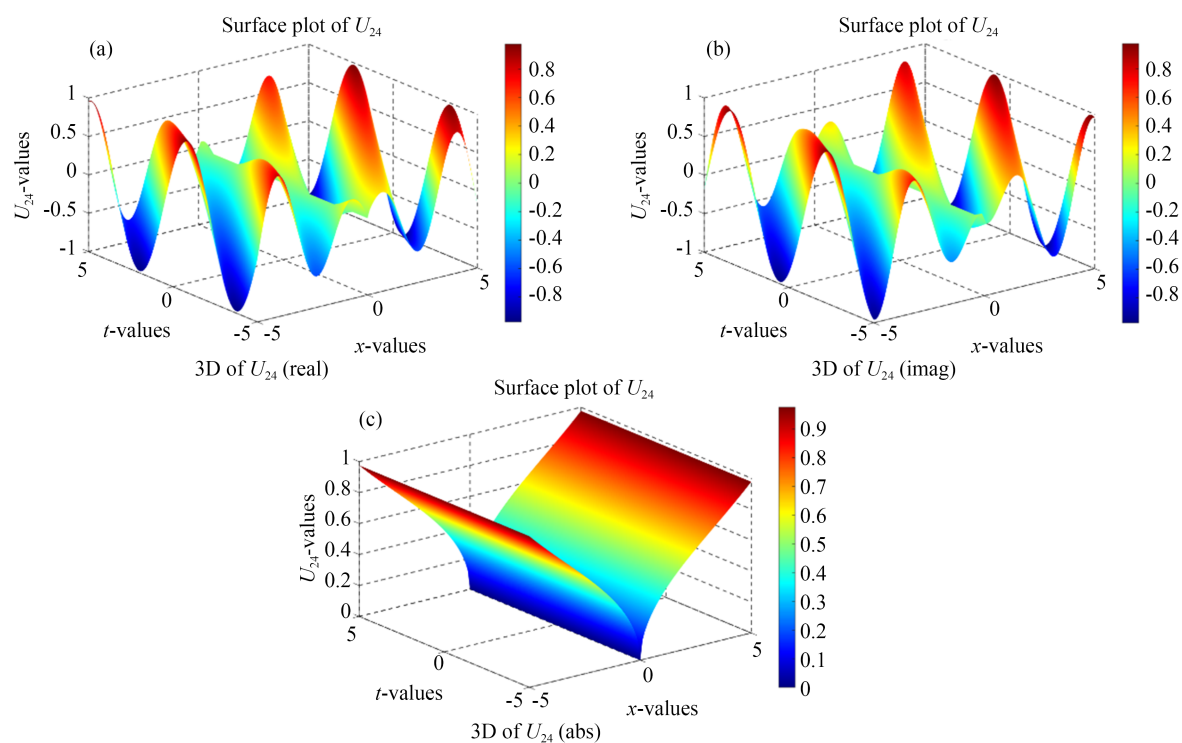


Figure 14. 3D plots of the solution U_{24}

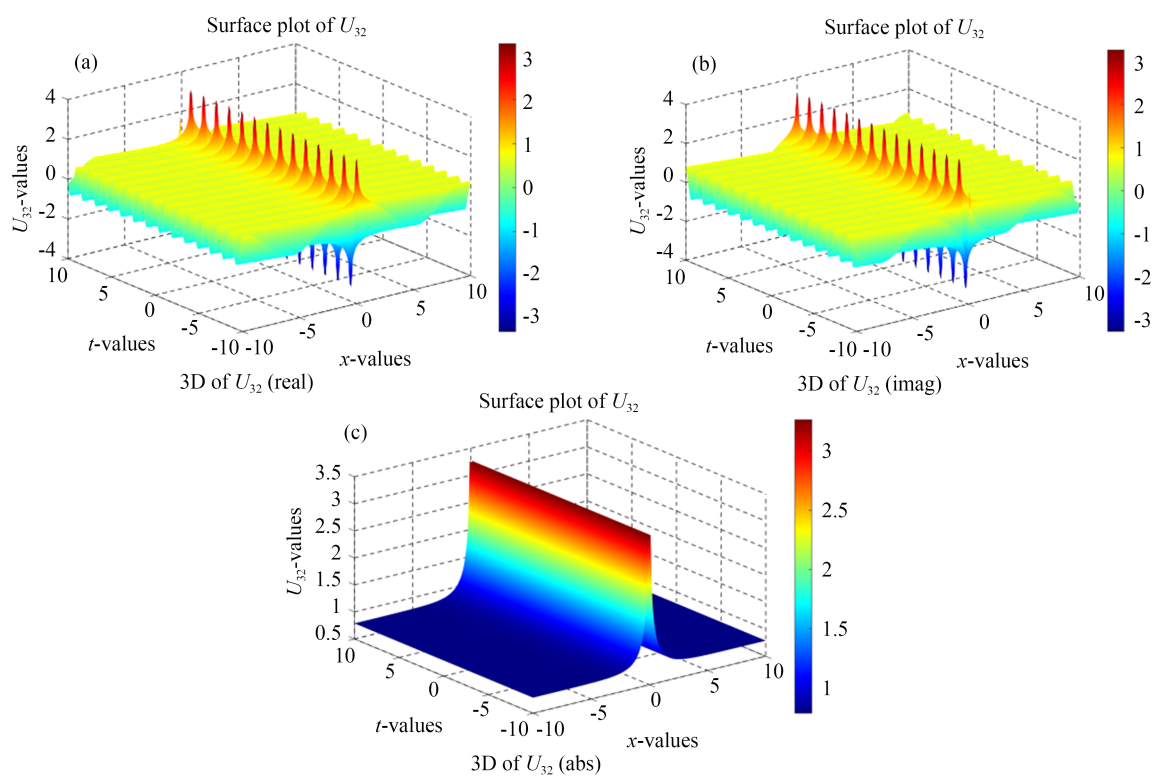


Figure 15. 3D plots of the solution U_{32}

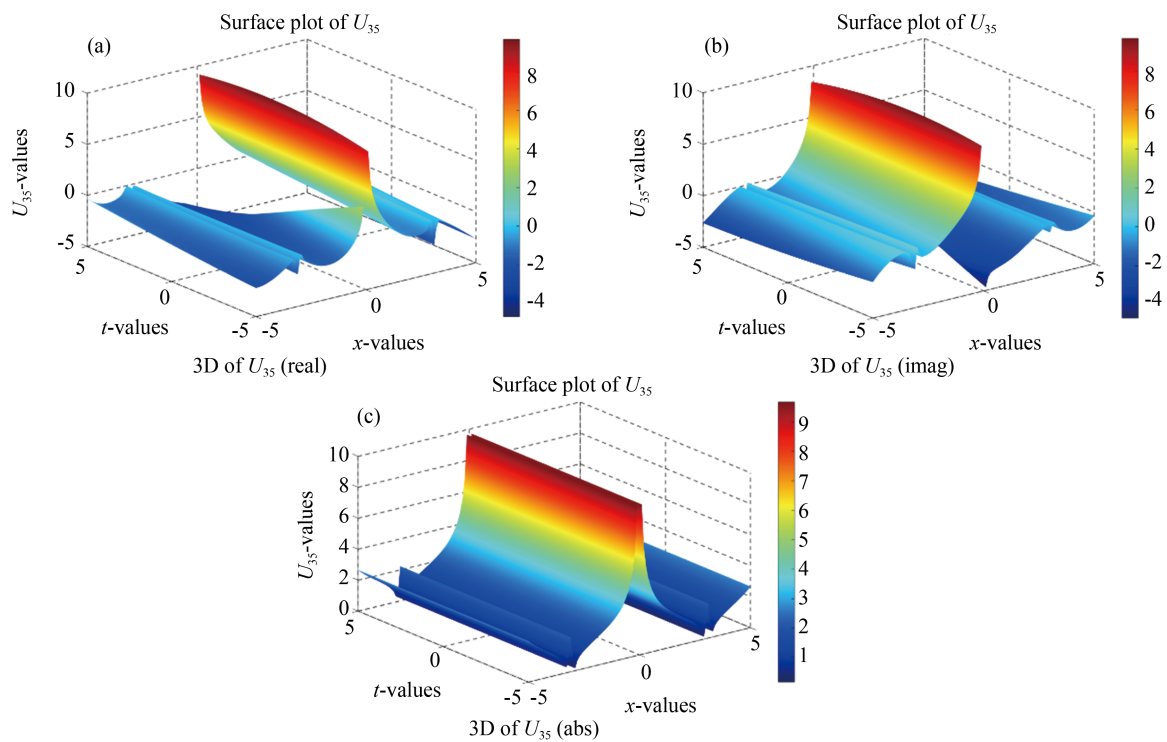


Figure 16. 3D plots of the solution U_{35}

6. MI for the nonlocal KE model

Whether bright or dark solitons occur depends on the presence of MI. The stability or instability of periodic bright and dark solitons, single solitons, and dark solitons for the nonlocal KE equation provides valuable insights into soliton dynamics in nonlinear sciences. The form contains the exact plane wave solutions:

$$U(x, t) = U_0 e^{i(\alpha x - \omega t)}, \quad (40)$$

where, U_0 , α and ω are related to the dispersion relation:

$$U^*(-x, t) = U_0 e^{i(\alpha x + \omega t)}. \quad (41)$$

$$U_t = -i\omega U_0 e^{i(\alpha x - \omega t)}. \quad (42)$$

$$U_x = i\alpha U_0 e^{i(\alpha x - \omega t)}. \quad (43)$$

$$U_{xx} = -\alpha^2 U_0 e^{i(\alpha x - \omega t)}. \quad (44)$$

$$UU^*(-x, t) = U_0^2 e^{i(\alpha x + \omega t)} e^{i(\alpha x - \omega t)} = U_0^2 e^{2i\alpha x}. \quad (45)$$

$$(UU^*(-x, t))_x = 2i\alpha U_0^2 e^{2i\alpha x}. \quad (46)$$

$$(UU^*(-x, t))U = U_0^2 e^{2i\alpha x} U_0 e^{i(\alpha x - \omega t)} = U_0^3 e^{i(3\alpha x - \omega t)}. \quad (47)$$

$$(UU^*(-x, t))^2 U = (U_0^2 e^{2i\alpha x})^2 U_0 e^{i(\alpha x - \omega t)} = U_0^5 e^{i(5\alpha x - \omega t)}. \quad (48)$$

$$U(UU^*(-x, t))_x = U_0 e^{i(\alpha x - \omega t)} 2i\alpha U_0^2 e^{2i\alpha x}. \quad (49)$$

$$U(UU^*(-x, t))_x = 2i\alpha U_0^3 e^{i(3\alpha x - \omega t)}. \quad (50)$$

Inserting Eqs. (42), (44), (47), (48) and (49) into Eq. (8), we have

$$\omega U_0 e^{i(\alpha x - \omega t)} - c_1 \alpha^2 U_0 e^{i(\alpha x - \omega t)} + c_2 U_0^3 e^{i(3\alpha x - \omega t)} + c_3 U_0^5 e^{i(5\alpha x - \omega t)} - c_4 2\alpha U_0^3 e^{i(3\alpha x - \omega t)} = 0. \quad (51)$$

In Eq. (51), higher-order harmonic terms exist that cannot generate MI, making the solution inconsistent. To obtain a consistent carrier waveform, we substitute $\alpha = 0$ in Eq. (51) leading to

$$(\omega + c_2 U_0^2 + c_3 U_0^4) e^{-i\omega t} = 0 \Rightarrow \omega = -(c_2 U_0^2 + c_3 U_0^4). \quad (52)$$

A small perturbation is introduced into the plane wave solution to analyze the wave's stability

$$U(x, t) = (U_0 + \delta U(x, t)) e^{i(\alpha x - \omega t)}, \quad (53)$$

Where $\delta U(x, t)$ is a small perturbation, i.e. $\delta U \ll 1$:

$$U^*(-x, t) = (U_0 + \delta U^*(-x, t)) e^{i(\alpha x + \omega t)}; \quad (54)$$

$$U_t(x, t) = (\delta U_t - i\omega \delta U) e^{i(\alpha x - \omega t)}; \quad (55)$$

$$U_{xx}(x, t) = (\delta U_{xx} + 2i\alpha \delta U_x - \alpha^2 \delta U) e^{i(\alpha x - \omega t)}; \quad (56)$$

$$(UU^*(-x, t))U = (2U_0^2 \delta U + U_0^2 \delta U^*(-x, t)) e^{i(3\alpha x - \omega t)}; \quad (57)$$

$$(UU^*(-x, t))^2 U = (3U_0^4 \delta U + 2U_0^4 \delta U^*(-x, t)) e^{i(5\alpha x - \omega t)}; \quad (58)$$

$$(UU^*(-x, t))_x = (2i\alpha(U_0^2 + U_0 \delta U + U_0 \delta U^*(-x, t)) + U_0 \delta U_x - U_0 \delta U_x^*) e^{2i\alpha x}; \quad (59)$$

$$U(UU^*(-x, t))_x = (2i\alpha(U_0^3 + U_0^2 \delta U + U_0^2 \delta U^*(-x, t)) + U_0^2 \delta U_x - U_0^2 \delta U_x^* + 2i\alpha U_0^2 \delta U) e^{i(3\alpha x - \omega t)}. \quad (60)$$

Retaining only terms $O(\delta U, \delta U^*)$ from Eqs. (55)-(60), and inserting them into Eq. (8), and we linearize around the unperturbed solutions and obtain:

$$\begin{aligned} & (i\delta U_t + \omega \delta U + c_1 [2i\alpha \delta U_x - \alpha^2 \delta U + \delta U_{xx}]) e^{i(\alpha x - \omega t)} + c_2 [2U_0^2 \delta U + U_0^2 \delta U^*(-x, t)] e^{i(3\alpha x - \omega t)} \\ & + c_3 [3U_0^4 \delta U + 2U_0^4 \delta U^*(-x, t)] e^{i(5\alpha x - \omega t)} \\ & + c_4 [iU_0^2 (\delta U_x - \delta U_x^*(-x, t)) - 2\alpha U_0^2 (\delta U + \delta U^*) - 2\alpha U_0^2 \delta U^*(-x, t)] e^{i(3\alpha x - \omega t)} = 0. \end{aligned} \quad (61)$$

For MI, higher-order harmonic terms are converted into similar carrier wave phase terms. Because, in MI or perturbation analysis, we usually assume the disturbance amplitude is small. In that regime, higher harmonics are much smaller in amplitude than the fundamental, so neglecting them gives an accurate approximation. For example, the linear stability analysis of plane waves is about small perturbations. Linearization automatically removes higher harmonics, because nonlinear interactions are dropped at leading order. If we keep all harmonics, we will get an infinite system of coupled equations. This system is generally not solvable in closed form without advanced tools such as Darboux transformation [17] or Riemann-Hilbert methods [18]. Besides MI is caused by resonant energy exchange between the carrier and its nearest sidebands, while higher harmonics represent secondary scattering processes that become important later.

Inserting $\alpha = 0$ into Eq. (61) for getting a similar carrier waveform, we get

$$\begin{aligned} & i\delta U_t + \omega \delta U + c_1 \delta U_{xx} + c_2 [2U_0^2 \delta U + U_0^2 \delta U^*(-x, t)] \\ & + (c_3 [3U_0^4 \delta U + 2U_0^4 \delta U^*(-x, t)] + c_4 [iU_0^2 (\delta U_x - \delta U_x^*(-x, t))]) e^{-i\omega t} = 0. \\ \Rightarrow & i\delta U_t + \omega \delta U + c_1 \delta U_{xx} + c_2 [2U_0^2 \delta U + U_0^2 \delta U^*(-x, t)] \\ & + c_3 [3U_0^4 \delta U + 2U_0^4 \delta U^*(-x, t)] + c_4 [iU_0^2 (\delta U_x - \delta U_x^*(-x, t))] = 0. \end{aligned} \quad (62)$$

We put the perturbation in the form

$$\delta U(x, t) = q_1 e^{i(\chi x - \eta t)} + q_2^* e^{-i(\chi x - \eta^* t)}. \quad (63)$$

Where χ and η represent the perturbed wave number and frequency, respectively. q_1 and q_2 correspond to the complex constant amplitudes and * complex conjugate:

$$\delta U_t = -i\eta q_1 e^{i(\chi x - \eta t)} + i\eta^* q_2^* e^{-i(\chi x - \eta^* t)}. \quad (64)$$

$$\delta U_{xx} = -\chi^2 q_1 e^{i(\chi x - \eta t)} - \chi^2 q_2^* e^{-i(\chi x - \eta^* t)}. \quad (65)$$

$$\delta U^*(-x, t) = q_1 e^{i(\chi x + \eta t)} + q_2^* e^{-i(\chi x + \eta^* t)}. \quad (66)$$

$$\delta U_x^*(-x, t) = i\chi q_1 e^{i(\chi x + \eta t)} - i\chi q_2^* e^{-i(\chi x + \eta^* t)}. \quad (67)$$

Inserting the values of Eqs. (63)-(67) into Eq. (62), we provide the following result:

$$\begin{aligned} & \eta q_1 e^{i(\chi x - \eta t)} - \eta^* q_2^* e^{-i(\chi x - \eta^* t)} + \omega q_1 e^{i(\chi x - \eta t)} + \omega q_2^* e^{-i(\chi x - \eta^* t)} - c_1 \chi^2 \left(q_1 e^{i(\chi x - \eta t)} + q_2^* e^{-i(\chi x - \eta^* t)} \right) \\ & + c_2 \left(2U_0^2 \left(q_1 e^{i(\chi x - \eta t)} + q_2^* e^{-i(\chi x - \eta^* t)} \right) + U_0^2 \left(q_1 e^{i(\chi x + \eta t)} + q_2^* e^{-i(\chi x + \eta^* t)} \right) \right) \\ & + c_3 \left(3U_0^4 \left(q_1 e^{i(\chi x - \eta t)} + q_2^* e^{-i(\chi x - \eta^* t)} \right) + 2U_0^4 \left(q_1 e^{i(\chi x + \eta t)} + q_2^* e^{-i(\chi x + \eta^* t)} \right) \right) \\ & + c_4 \left(iU_0^2 \left(i\chi q_1 e^{i(\chi x - \eta t)} - i\chi q_2^* e^{-i(\chi x - \eta^* t)} - i\chi q_1 e^{i(\chi x + \eta t)} + i\chi q_2^* e^{-i(\chi x + \eta^* t)} \right) \right) = 0. \end{aligned} \quad (68)$$

We get the linear equation from (68) as follows:

$$[\eta + \omega - c_1 \chi^2 + 2c_2 U_0^2 + 3c_3 U_0^4 - c_4 U_0^2 \chi] q_1 e^{i(\chi x - \eta t)} + [U_0^2 c_2 + 2c_3 U_0^4 - c_4 U_0^2 \chi] q_2^* e^{-i(\chi x + \eta^* t)} = 0. \quad (69)$$

$$[c_2 U_0^2 + 2c_3 U_0^4 + c_4 U_0^2 \chi] q_1 e^{i(\chi x + \eta t)} + [-\eta + \omega - c_1 \chi^2 + 2c_2 U_0^2 + 3c_3 U_0^4 + c_4 U_0^2 \chi] q_2^* e^{-i(\chi x - \eta^* t)} = 0. \quad (70)$$

The above equations can be written in matrix form

$$\begin{pmatrix} \eta + A & C \\ B & -\eta + D \end{pmatrix} \begin{pmatrix} q_1 \\ q_2^* \end{pmatrix} = \begin{pmatrix} 0 \\ 0 \end{pmatrix}. \quad (71)$$

Where,

$$A = \omega - c_1 \chi^2 + 2c_2 U_0^2 + 3c_3 U_0^4 - c_4 U_0^2 \chi,$$

$$B = U_0^2 c_2 + 2c_3 U_0^4 + c_4 U_0^2 \chi,$$

$$C = U_0^2 c_2 + 2c_3 U_0^4 - c_4 U_0^2 \chi,$$

$$D = \omega - c_1 \chi^2 + 2c_2 U_0^2 + 3c_3 U_0^4 + c_4 \chi U_0^2.$$

If the determinant of the above matrix disappears, the solution of Eq. (71) is nontrivial and yields the following equation:

$$\eta^2 - \eta(D - A) - AD + BC = 0. \quad (72)$$

Solving the equation, we achieve:

$$\eta = \frac{(D - A) \pm \sqrt{(D + A)^2 - 4BC}}{2}. \quad (73)$$

From the characteristics of the equation (73), we can conclude the stability of bright, dark, periodic, and singular solitons for the nonlocal KE equation. Instability arises when the dispersion relation yields an imaginary frequency component, indicating exponential growth of perturbations. Since the perturbation grows exponentially, the plane wave solution is unstable. As a consequence, the MI attains for the nonlocal KE equation:

$$H(\eta) = \text{Im}(\eta) = \frac{\sqrt{(D + A)^2 - 4BC}}{2}. \quad (74)$$

Figures 17a to 17f illustrate the gain spectrum for the nonlocal Kundu-Eckhaus equation for the values $c_1 = 1.1$, $c_4 = 1$, where $-5 \leq x \leq 5$ and $-5 \leq U_0 \leq 5$.

Figures 18a to 18c represent the gain spectrum for the nonlocal Kundu-Eckhaus equation for $c_2 = 1$, $c_3 = 1$, where $-5 \leq x \leq 5$ and $-5 \leq U_0 \leq 5$.

Figures 19a to 19c offer the gain spectrum for the nonlocal Kundu-Eckhaus equation for the constants $c_2 = 10$, $c_3 = 10$, where $-5 \leq x \leq 5$ and $-5 \leq U_0 \leq 5$.

The MI of bright, dark, periodic, and singular solitons for the nonlocal KE equation is determined from Eq. (73). Moreover, the gain spectra are plotted using the following parameters c_1 , c_2 , c_3 and c_4 as demonstrated in Figures 17 to 19. In the gain spectrum, the scale on the x-axis is the perturbed wave number x , and the amplitude is U_0 along the y-axis. Figures 17a to 17f demonstrate the choice of the parameters $c_1 = 1.1$, $c_4 = 1$ and the others are stored in the figures, where $-5 \leq U_0 \leq 5$. The gain spectrum shows that the stable region is concentrated near the center while the unstable region appears at the corner, indicated by yellow. As the parameter c_2 and c_3 increase, the stable region expands (shown in dark blue), while the unstable region shrinks (yellow regions in the left- and right-hand sides). Figures 18a to 18c depict the stable and unstable areas for increasing the values of c_1 and c_4 , where c_2 and c_3 values are 1. Figure 19a shows that, when $c_1 = 0$, and $c_4 = 0$, here it appears that the stable region is about the entire space with a little unstable region in the upper and lower sides. Slightly promoting the values of c_1 and c_4 , the presence of an unstable region appears as a straight line in the middle part of the plot, except for some areas on that line. After that, in Figure 19c, when c_1 , c_4 values are reached at 40, the amount of unstable area increases and the stable area decreases. At the linear stage of instability, the dynamics are governed entirely by the nearest sidebands, which capture the threshold and growth rate of MI. The MI analysis here retains only the fundamental modulation sidebands. While this approximation provides the correct leading-order threshold and gain profile, it omits higher-order harmonic interactions arising from nonlocal and PT-symmetric terms. Therefore, the present MI results are interpreted as first-order indicators of instability. A more complete picture of the nonlinear stage

of MI would require the inclusion of higher harmonics or direct numerical simulations, which we leave for future work. In this work, we demonstrate the stability or instability of the soliton for the nonlocal nonlinear KE equation to support the optical transmission manufacturing industry or optical phenomena.

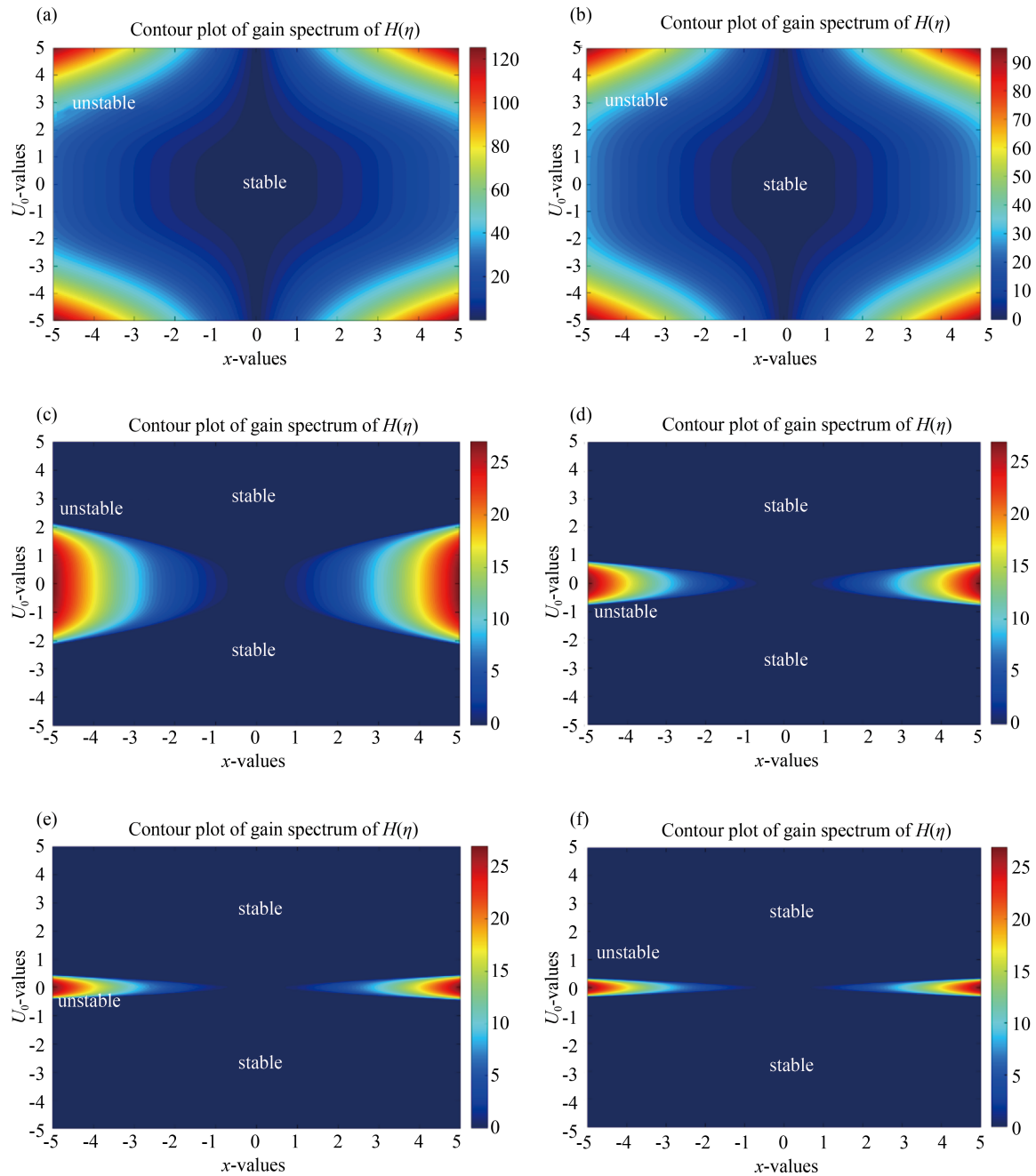


Figure 17. (a) $c_2 = 0.001, c_3 = 0.001$; (b) $c_2 = 0.01, c_3 = 0.01$; (c) $c_2 = 0.5, c_3 = 0.5$; (d) $c_2 = 10, c_3 = 10$; (e) $c_2 = 50, c_3 = 50$; (f) $c_2 = 100, c_3 = 100$

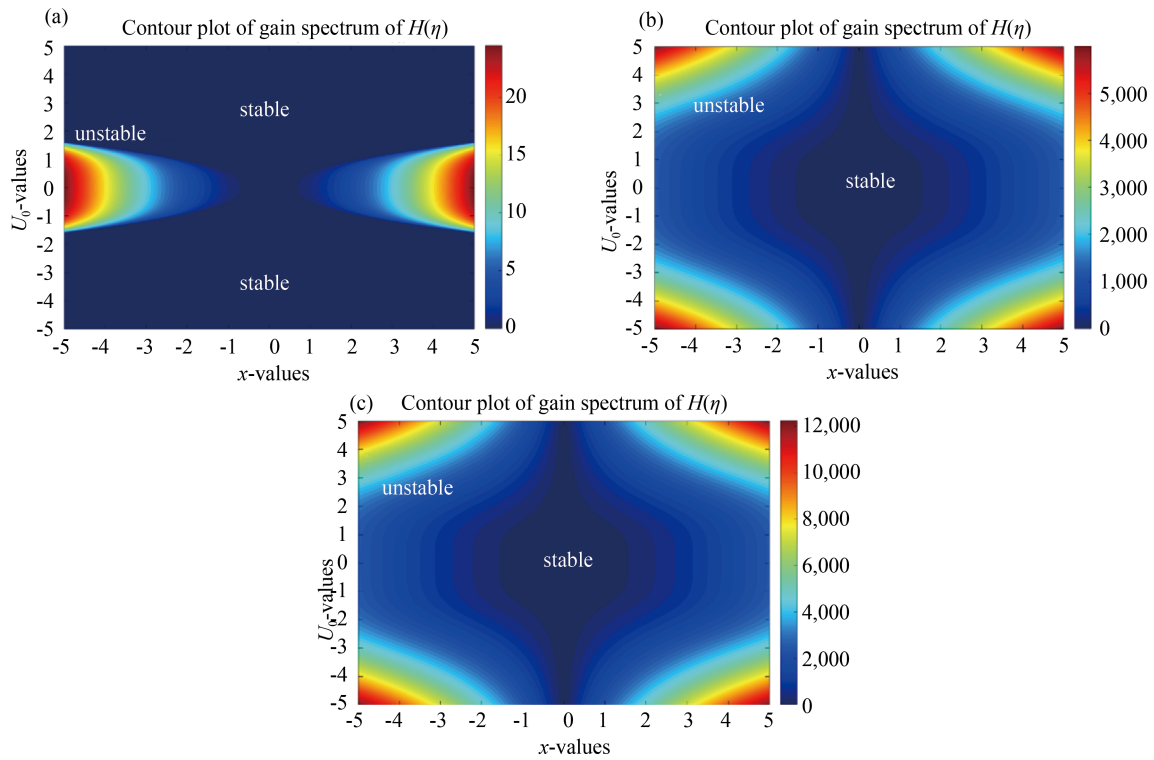


Figure 18. (a) $c_1 = 1, c_4 = 1$; (b) $c_1 = 50, c_4 = 50$; (c) $c_1 = 100, c_4 = 100$

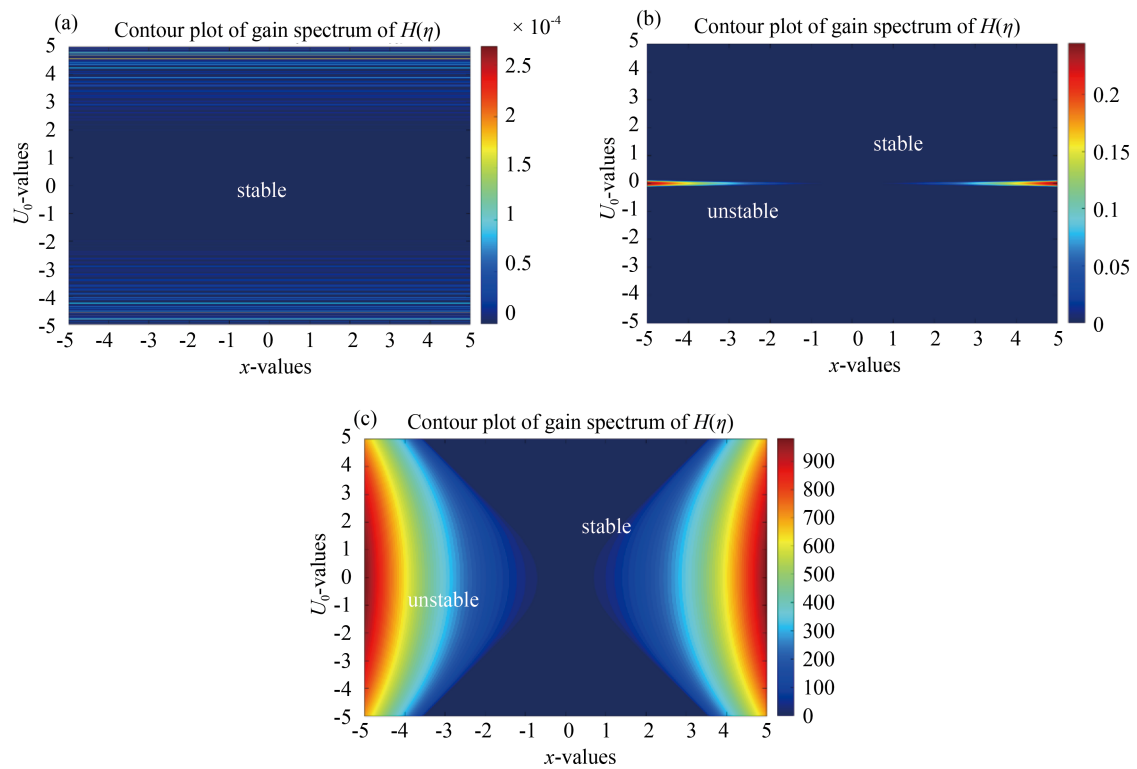


Figure 19. (a) $c_1 = 0, c_4 = 0$; (b) $c_1 = 0.01, c_4 = 0.01$; (c) $c_1 = 40, c_4 = 40$

7. Comparison with established methods

To situate our present work within a wide range of landscapes of exact solution techniques for nonlocal equations, it is instructive to compare our approach with established methods. The Hirota bilinear method transforms nonlinear equations into bilinear forms, enabling the systematic construction of multi-soliton solutions [16]. It primarily works for local equations and often requires intricate algebraic manipulations for nonlocal variants. Our method simplifies the application to nonlocal equations without bilinearization. The Darboux transformation [17] systematically generates new solutions involving intensive algebraic computations. Although powerful, it depends on a known seed solution. In contrast, the present method constructs exact solutions directly without seeds or iterative steps. And the Riemann-Hilbert approach formulates integrable systems as analytic boundary-value problems, allowing for a systematic derivation of soliton solutions [18]. Despite its generality, it often involves complex analytical machinery and can be challenging to implement for nonlocal equations. In contrast, the present method directly constructs exact solutions for nonlocal systems without requiring bilinearization, seed solutions, or complex analytic machinery. This not only simplifies the derivation process but also extends the applicability of solution techniques to a wider class of nonlocal equations, highlighting both the novelty and practical significance of our approach.

8. Conclusions and future

This study extended the nonlocal Kundu-Eckhaus equation by incorporating nonlocality and PT-symmetric terms to construct a generalized framework suitable for nonlinear complex physical phenomena, especially in optical birefringent fibers. By applying the $\frac{AG'}{GE}$ method, we obtain fifteen exact solutions, among which five were plotted to visualize the solution behaviors of dark, bright, periodic, multi-periodic, and singular solitons. A broad set of exact analytical solutions demonstrates the effectiveness of the applied method in handling complex nonlinear structures. We performed linear stability analysis to identify the conditions responsible for MI. We carefully analyzed how cubic and quartic nonlinearities influence the MI of soliton solutions of the nonlocal Kundu-Eckhaus equation. The inclusion of nonlocality and PT-symmetric terms in the KE equation alters the gain profile and affects the emergence and evolution of MI. The results may provide insights into MI, solution interactions in birefringent fibers, and PT-symmetric waveguides, all essential for efficient signal transmission. This study develops a direct analytical framework for both nonlocality and PT symmetry into the Kundu-Eckhaus equation. By applying the $\frac{AG'}{GE}$ method, we derived fifteen distinct classes of exact soliton solutions—including dark, bright, periodic, multi-periodic, and singular types along with their graphical representations. Compared to classical methods such as the Hirota bilinear approach, Darboux transformation, and Riemann-Hilbert problem, the proposed method avoids complex bilinearization, seed dependence, and heavy analytic procedures. Solutions are verified analytically and validated through numerical simulations confirming stability and dynamic evolution. Furthermore, a detailed linear stability and MI analysis was conducted, highlighting how cubic and quintic nonlinearities influence soliton stability. The approach offers a simple, efficient, and broadly applicable alternative for studying nonlocal integrable systems.

This research may extend the study of higher-dimensional and fractional-order PDEs, allowing a broader understanding of complex spatio-temporal behaviors in nonlocal systems. Incorporating higher-order perturbation terms into MI analysis could provide a refined understanding of stability regimes. The proposed $\frac{AG'}{GE}$ approach can also be generalized to other nonlocal or coupled nonlinear PDEs to investigate multi-component interactions, cross-modulation phenomena, and energy exchange mechanisms, while advanced numerical simulations will be essential for validating analytical results and linking them with experimental observations. This will create a bridge between theoretical insights and potential experimental realizations.

Conflict of interest

The authors declare no competing financial interest.

References

- [1] Abdalla M, Roshid MM, Uddin M, Ullah MS. Analysis MI and parametric effect on soliton solutions for M-fractional Landau-Ginzburg-Higgs (LGH) equation through two analytic methods. *Fractal and Fractional*. 2025; 9(3): 154. Available from: <https://doi.org/10.3390/fractalfract9030154>.
- [2] Ablowitz MJ, Musslimani ZH. Integrable nonlocal nonlinear equations. *Studies in Applied Mathematics*. 2017; 139(1): 7-59. Available from: <https://doi.org/10.1111/sapm.12153>.
- [3] Ablowitz MJ, Musslimani ZH. Integrable nonlocal nonlinear Schrödinger equation. *Physical Review Letters*. 2013; 110(6): 064105. Available from: <https://doi.org/10.1103/PhysRevLett.110.064105>.
- [4] Gilson CR, Nimmo JJC, Willox R. A $(2 + 1)$ -dimensional generalization of the AKNS shallow water wave equation. *Physics Letters A*. 1993; 180(4-5): 337-345. Available from: [https://doi.org/10.1016/0375-9601\(93\)91187-A](https://doi.org/10.1016/0375-9601(93)91187-A).
- [5] Bender CM, Boettcher S. Real spectra in non-Hermitian Hamiltonians having PT symmetry. *Physical Review Letters*. 1998; 80(24): 5243. Available from: <https://doi.org/10.1103/PhysRevLett.80.5243>.
- [6] Bender CM, Boettcher S, Meisinger PN. PT-symmetric quantum mechanics. *Journal of Mathematical Physics*. 1999; 40(5): 2201-2229. Available from: <https://doi.org/10.1063/1.532860>.
- [7] Song Y, Shi X, Wu C, Tang D, Zhang H. Recent progress of study on optical solitons in fiber lasers. *Applied Physics Reviews*. 2019; 6(2). Available from: <https://doi.org/10.1063/1.5091811>.
- [8] Bender CM, Berntson BK, Parker D, Samuel E. Observation of PT phase transition in a simple mechanical system. *American Journal of Physics*. 2013; 81(3): 173-179. Available from: <https://doi.org/10.1119/1.4789549>.
- [9] Sarma AK, Miri MA, Musslimani ZH, Christodoulides DN. Continuous and discrete Schrödinger systems with parity-time-symmetric nonlinearities. *Physical Review E*. 2014; 89(5): 052918. Available from: <https://doi.org/10.1103/PhysRevE.89.052918>.
- [10] Lin Z, Ramezani H, Eichelkraut T, Kottos T, Cao H, Christodoulides DN. Unidirectional invisibility induced by PT-symmetric periodic structures. *Physical Review Letters*. 2011; 106(21): 213901. Available from: <https://doi.org/10.1103/PhysRevLett.106.213901>.
- [11] Tai K, Hasegawa A, Tomita A. Observation of modulational instability in optical fibers. *Physical Review Letters*. 1986; 56(2): 135. Available from: <https://doi.org/10.1103/PhysRevLett.56.135>.
- [12] Arnous AH, Ullah MZ, Moshokoa SP, Zhou Q, Triki H, Mirzazadeh M, et al. Optical solitons in birefringent fibers with modified simple equation method. *Optik*. 2017; 130: 996-1003. Available from: <https://doi.org/10.1016/j.ijleo.2016.11.101>.
- [13] Ma WX. Nonlocal PT-symmetric integrable equations and related Riemann-Hilbert problems. *Partial Differential Equations in Applied Mathematics*. 2021; 4: 100190. Available from: <https://doi.org/10.1016/j.padiff.2021.100190>.
- [14] Menyuk CR. Solitons in birefringent optical fibers and polarization mode dispersion. *Optics Communications*. 2024; 550: 129841. Available from: <https://doi.org/10.1016/j.optcom.2023.129841>.
- [15] Younis M, Sulaiman TA, Bilal M, Rehman SU, Younas U. MI analysis, optical and other solutions to the modified nonlinear Schrödinger equation. *Communications in Theoretical Physics*. 2020; 72(6): 065001. Available from: <https://doi.org/10.1088/1572-9494/ab7ec8>.
- [16] Zhou Y, Ma WX. Complexiton solutions to soliton equations by the Hirota method. *Journal of Mathematical Physics*. 2017; 58(10). Available from: <https://doi.org/10.1063/1.4996358>.
- [17] Riaz HWA, Lin J. Darboux transformation for a semi-discrete matrix coupled dispersionless system. *Applied Mathematics Letters*. 2024; 158: 109217. Available from: <https://doi.org/10.1016/j.aml.2024.109217>.
- [18] Gerdjikov VS, Stefanov AA. Riemann-Hilbert problems, polynomial Lax pairs, integrable equations and their soliton solutions. *Symmetry*. 2023; 15(10): 1933. Available from: <https://doi.org/10.3390/sym15101933>.
- [19] Bevacqua MT, Crocco L, Di Donato L, Isernia T. An algebraic solution method for nonlinear inverse scattering. *IEEE Transactions on Antennas and Propagation*. 2014; 63(2): 601-610. Available from: <https://doi.org/10.1109/TAP.2014.2382114>.

- [20] Alam MN, Akbar MA, Mohyud-Din ST. A novel (G'/G) -expansion method and its application to the Boussinesq equation. *Chinese Physics B*. 2013; 23(2): 020203. Available from: <https://doi.org/10.1088/1674-1056/23/2/020203>.
- [21] Vajda S, Godfrey KR, Rabitz H. Similarity transformation approach to identifiability analysis of nonlinear compartmental models. *Mathematical Biosciences*. 1989; 93(2): 217-248. Available from: [https://doi.org/10.1016/0025-5564\(89\)90024-2](https://doi.org/10.1016/0025-5564(89)90024-2).
- [22] Bansal A, Biswas A, Zhou Q, Babatin MM. Lie symmetry analysis for cubic-quartic nonlinear Schrödinger's equation. *Optik*. 2018; 169: 12-15. Available from: <https://doi.org/10.1016/j.ijleo.2018.05.030>.
- [23] Moghaddam MY, Asgari A, Yazdani H. Exact travelling wave solutions for the generalized nonlinear Schrödinger (GNLS) equation with a source by extended tanh-coth, sine-cosine and Exp-function methods. *Applied Mathematics and Computation*. 2009; 210(2): 422-435. Available from: <https://doi.org/10.1016/j.amc.2009.01.002>.
- [24] Fan E, Zhang J. Applications of the Jacobi elliptic function method to special-type nonlinear equations. *Physics Letters A*. 2002; 305(6): 383-392. Available from: [https://doi.org/10.1016/S0375-9601\(02\)01516-5](https://doi.org/10.1016/S0375-9601(02)01516-5).
- [25] Alam MN. Simulation of wave solutions of mathematical model representing electrical engineering by using an analytical technique. *Journal of Mechanics of Continua and Mathematical Science*. 2023; 18(1). Available from: <https://doi.org/10.26782/jmcms.2023.01.00003>.
- [26] Park QH, Shin HJ. Painlevé analysis of the coupled nonlinear Schrödinger equation for polarized optical waves in an isotropic medium. *Physical Review E*. 1999; 59(2): 2373. Available from: <https://doi.org/10.1103/PhysRevE.59.2373>.
- [27] Attaullah, Shakeel M, Ahmad B, Shah NA, Chung JD. Solitons solution of Riemann wave equation via modified exp function method. *Symmetry*. 2022; 14(12): 2574. Available from: <https://doi.org/10.3390/sym14122574>.
- [28] Sirisubtawee S, Koonprasert S, Sungnul S. Some applications of the $(G'/G, 1/G)$ -expansion method for finding exact traveling wave solutions of nonlinear fractional evolution equations. *Symmetry*. 2019; 11(8): 952. Available from: <https://doi.org/10.3390/sym11080952>.
- [29] Akram G, Arshed S, Sadaf M, Sameen F. The generalized projective Riccati equations method for solving quadratic-cubic conformable time-fractional Klien-Fock-Gordon equation. *Ain Shams Engineering Journal*. 2022; 13(4): 101658. Available from: <https://doi.org/10.1016/j.asej.2021.101658>.
- [30] Wang M, Zhou Y, Li Z. Application of a homogeneous balance method to exact solutions of nonlinear equations in mathematical physics. *Physics Letters A*. 1996; 216(1-5): 67-75. Available from: [https://doi.org/10.1016/0375-9601\(96\)00283-6](https://doi.org/10.1016/0375-9601(96)00283-6).
- [31] Mathanaranjan T. Soliton solutions of deformed nonlinear Schrödinger equations using ansatz method. *International Journal of Applied and Computational Mathematics*. 2021; 7(4): 159. Available from: <https://doi.org/10.1007/s40819-021-01099-y>.
- [32] Mahmood A, Srivastava HM, Abbas M, Abdullah FA, Mohammed PO, Baleanu D, et al. Optical soliton solutions of the coupled Radhakrishnan-Kundu-Lakshmanan equation by using the extended direct algebraic approach. *Heliyon*. 2023; 9(10). Available from: <https://doi.org/10.1016/j.heliyon.2023.e20852>.
- [33] Eslami M, Matinfar M, Asghari Y, Rezazadeh H, Abduridha SAJ. Diverse exact soliton solutions for three distinct equations with conformable derivatives via expa function technique. *Optical and Quantum Electronics*. 2024; 56(5): 846. Available from: <https://doi.org/10.1007/s11082-024-06518-0>.
- [34] Mirhosseini-Alizamini SM, Rezazadeh H, Eslami M, Mirzazadeh M, Korkmaz A. New extended direct algebraic method for the Tzitzica type evolution equations arising in nonlinear optics. *Computational Methods for Differential Equations*. 2020; 8(1): 28-53. Available from: <https://doi.org/10.22034/cmde.2019.9472>.
- [35] Osman MS, Ali KK, Gómez-Aguilar JF. A variety of new optical soliton solutions related to the nonlinear Schrödinger equation with time-dependent coefficients. *Optik*. 2020; 222: 165389. Available from: <https://doi.org/10.1016/j.ijleo.2020.165389>.
- [36] Kabir MM, Khajeh A, Abdi Aghdam E, Yousefi Koma A. Modified Kudryashov method for finding exact solitary wave solutions of higher-order nonlinear equations. *Mathematical Methods in the Applied Sciences*. 2011; 34(2): 213-219. Available from: <https://doi.org/10.1002/mma.1349>.
- [37] Kumar D, Hosseini K, Samadani F. The sine-Gordon expansion method to look for the traveling wave solutions of the Tzitzéica type equations in nonlinear optics. *Optik*. 2017; 149: 439-446. Available from: <https://doi.org/10.1016/j.ijleo.2017.09.066>.

- [38] Galaktionov VA, Svirshchevskii SR. *Exact Solutions and Invariant Subspaces of Nonlinear Partial Differential Equations in Mechanics and Physics*. Chapman and Hall/CRC; 2006. Available from: <https://doi.org/10.1201/9781420011623>.
- [39] Cinar M, Secer A, Ozisik M, Bayram M. Derivation of optical solitons of dimensionless Fokas-Lenells equation with perturbation term using Sardar sub-equation method. *Optical and Quantum Electronics*. 2022; 54(7): 402. Available from: <https://doi.org/10.1007/s11082-022-03819-0>.
- [40] Vitanov NK, Dimitrova ZI, Kantz H. Modified method of simplest equation and its application to nonlinear PDEs. *Applied Mathematics and Computation*. 2010; 216(9): 2587-2595. Available from: <https://doi.org/10.1016/j.amc.2010.03.102>.
- [41] Khuri SA, Wazwaz AM. Optical solitons and traveling wave solutions to Kudryashov's equation. *Optik*. 2023; 279: 170741. Available from: <https://doi.org/10.1016/j.ijleo.2023.170741>.
- [42] Roshid MM, Rahman MM. Bifurcation analysis, MI and optical soliton solutions and their wave propagation insights to the variable coefficient nonlinear Schrödinger equation with Kerr law nonlinearity. *Nonlinear Dynamics*. 2024; 112(18): 16355-16377. Available from: <https://doi.org/10.1007/s11071-024-09872-6>.
- [43] Galle F, Brun PT. Fluid dynamic instabilities: theory and application to pattern forming in complex media. *Philosophical Transactions of the Royal Society A: Mathematical, Physical and Engineering Sciences*. 2017; 375(2093): 20160155. Available from: <https://doi.org/10.1098/rsta.2016.0155>.
- [44] Parasuraman E. Stability of kink, anti kink and dark soliton solution of nonlocal Kundu-Eckhaus equation. *Optik*. 2023; 290: 171279. Available from: <https://doi.org/10.1016/j.ijleo.2023.171279>.